CHALMERS

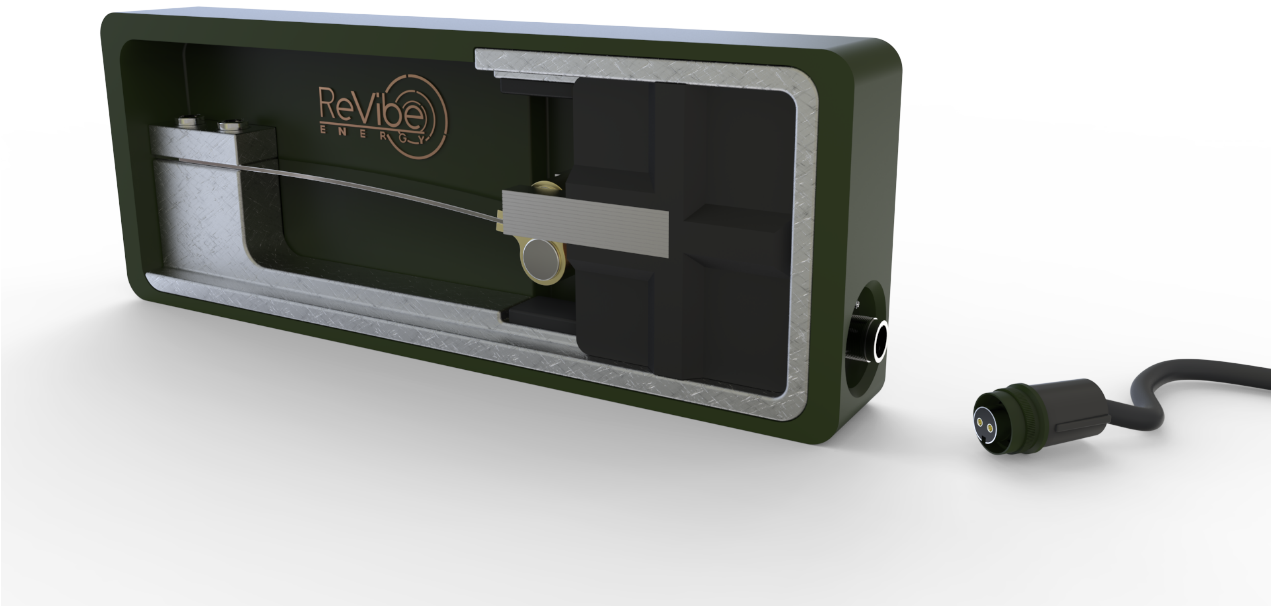

Design and verification of vibration energy harvester

An early product development project at a start-up company

Master's thesis in Product Development

FREDRIK HENNINGSEN
ANDREAS JOSEFSSON

Department of Applied Mechanics
Division of Dynamics
CHALMERS UNIVERSITY OF TECHNOLOGY
Göteborg, Sweden 2014
Master's thesis 2014:28

MASTER'S THESIS IN PRODUCT DEVELOPMENT

Design and verification of vibration energy harvester

An early product development project at a start-up company

FREDRIK HENNINGSEN
ANDREAS JOSEFSSON

Department of Applied Mechanics
Division of Dynamics
CHALMERS UNIVERSITY OF TECHNOLOGY

Göteborg, Sweden 2014

Design and verification of vibration energy harvester
An early product development project at a start-up company
FREDRIK HENNINGSEN
ANDREAS JOSEFSSON

Master's thesis 2014:28
ISSN 1652-8557
Department of Applied Mechanics
Division of Dynamics
Chalmers University of Technology
SE-412 96 Göteborg
Sweden
Telephone: +46 (0)31-772 1000

Cover:
Render of second generation prototype with casing

Chalmers Reproservice
Göteborg, Sweden 2014

Design and verification of vibration energy harvester
An early product development project at a start-up company
Master's thesis in Product Development
FREDRIK HENNINGSEN
ANDREAS JOSEFSSON
Department of Applied Mechanics
Division of Dynamics
Chalmers University of Technology

Abstract

Wireless Sensor Networks are becoming more and more popular as a means for monitoring civil structures and machine health. With increased size of these networks, using batteries for power supply is becoming unsustainable in terms of both maintenance cost and environmental impact. An alternative power supply to batteries is so-called Energy Harvesting, a principle based on scavenging ambient energy. Energy Harvesting Foundation is a Swedish start-up company developing an energy harvesting device converting vibrations into electricity. This project has consisted in laying a basis for optimising this technology as well as creating a methodology for evaluating its potential in various environments.

In their market research, Energy Harvesting Foundation has identified railway cargo freight wagons as an interesting area of application for their product. A company operating within this sector requested a prototype for testing with their wireless sensor system by the end of March 2014. Meeting this demand has been one of the main goals of the project. By digging into the fundamentals of vibrations and electromagnetism some designs have be created. These where manufactured and tested on a shaking device before a final prototype could be delivered to the customer.

For effectively evaluating vibration characteristics and enabling easy configuration for certain applications in the future, another part of the project has consisted in developing a simplified virtual model. For an example, this model could be used for predicting the performance of the harvesting device given a certain vibration pattern. Finally, fatigue in combination with functional analysis have been performed in order to ascertain a competitive lifetime of the device while producing sufficient power.

Keywords: Vibration Energy Harvesting, Wireless Sensor Networks, Design of Experiments, Safe Life Design, Early Product Development, Resonance Behaviour

Preface

This master's thesis was conducted at Chalmers University of Technology as a part of the Product Development Master's programme. The project has been carried out during the spring of 2014 on behalf of the start-up company Energy Harvesting Foundation.

We would like to thank Energy Harvesting Foundation for their trust in our ability to proceed their product development work and their support throughout our journey. We would also like to thank our supervisor Mikael Enelund for his guidance and important input. Other people that we would like to thank for their contributions are Tore Vernersson, Jan Möller, Per Cederwall, and Jan Bragée.

Göteborg, June 2014

Fredrik Henningsen
Andreas Josefsson

Contents

Abbreviations and Nomenclature

VEH = Vibration Energy Harvester
WSN = Wireless Sensor Network
PTP = Peak to Peak
RMS = Root Mean Square
$SDOF$ = Single Degree of Freedom
FEM = Finite Element Method
DOE = Design of Experiments

k = Spring stiffness coefficient
c = Spring damping coefficient
f = Frequency [Hz]
ω = Angular frequency [rad/s]
E = Young's modulus [GPa]
ξ = Damping coefficient
P = Power [W]
Φ = Magnetic flux [Wb]
B = Magnetic flux density [T]
H = Magnetic field intensity [A/m]
μ = Permeability [Wb/Am]
M = Magnetisation [kA/m]
U = Voltage [V]
$\mathcal{R}$ = Magnetic reluctance [1/H]
a = Acceleration [m/s^2]
R = Resistance [Ω]

1

Introduction

This chapter briefly describes the incentives for developing energy harvesting solutions as well as introducing Energy Harvesting Foundation as a start-up company within this market segment. It also phrases the purpose and the scope of this project.

1.1 WSN and energy harvesting

A wireless sensor network (WSN) is an arrangement of autonomous sensors for monitoring or controlling of physical or environmental conditions [1]. Along with the development of smaller and more power-efficient electronics and advancements in wireless communication, WSN technology has increased in popularity and new applications have developed. Today, some common areas of use for wireless networks are detection and characterisation of defects in civil structures, industrial process monitoring, and security applications [2], [3].

The sensor nodes that comprise a WSN are typically placed in remote locations where wired power is not available and thus a known problem is how to provide these nodes with sufficient of power. Using batteries for energy is a well-established practice but is only a viable option if the battery will survive the lifetime of the node [4]. In most cases, using batteries will come with a need for periodical recharge and/or replacement, which makes the use of batteries economically unsustainable for large networks with many nodes.

An alternative way of powering a WSN is to extract the energy needed from the environment. This is known as energy harvesting or scavenging and it means that ambient energy sources such as mechanical, thermal, or solar energy are converted into productive electricity [5]. One of the more common energy harvesting devices used today is the solar cell, which in some cases is supplying power directly and in other applications acts as a charger for batteries and thereby extend the life of the same [2].

The incentive for developing energy harvesting solutions is not only economical. For example, eliminating the need for maintenance will not only come with a decreased disposal of batteries thus a positive impact on the environment, but also a “place-and-forget” capability of nodes allowing to fully integrate them in structures [6]. Also, the combination of harvesting technology together with sensor node makes a complete package that is easy and cheap to retrofit.

Power generation from mechanical energy is one of the harvesting research areas that have been studied the most due to its high availability in technical environments [7]. Mechanical energy is typically expressed in form of vibrations, which are oscillations about an equilibrium position [8]. Low-level vibrations are available in many different environments ranging from regular home appliances such as washing machines and microwave ovens to roads and bridges.

According to Roundy, Wright, and Rabaey, there are three fundamental mechanisms by which vibrations can be converted into electrical energy: electromagnetic, electrostatic, and piezoelectric [2]. Electromagnetic conversion means that a coil and an magnetic field are moved relative to each other in order to induce a current in the coil. The second technology is also based on the relative motion of two objects, here being two conductors in a dielectric. Piezoelectric conversion is based on mechanically stressing piezoelectric materials in order to produce a voltage.

1.2 Energy Harvesting Foundation

Energy Harvesting Foundation (fictive name) is a Swedish start-up company developing a new kind of vibration energy harvester (VEH) for powering wireless sensor networks. The technology was originally developed at Saab Training and Simulation Systems and stems from the need of reliable and durable energy sources that can be used in off-grid areas. It works through converting mechanical vibrations into electricity using the electromagnetic mechanism mentioned above. This is achieved by the use of two main components: a cantilevered beam with magnets attached to its end, and a copper coil (see Figure 1.1). When subjected to vibrations, the beam will be affected by the kinetic energy and start oscillating. The magnetic field surrounding the coil will thereby change back and forth and thus a current will be induced in the coil.

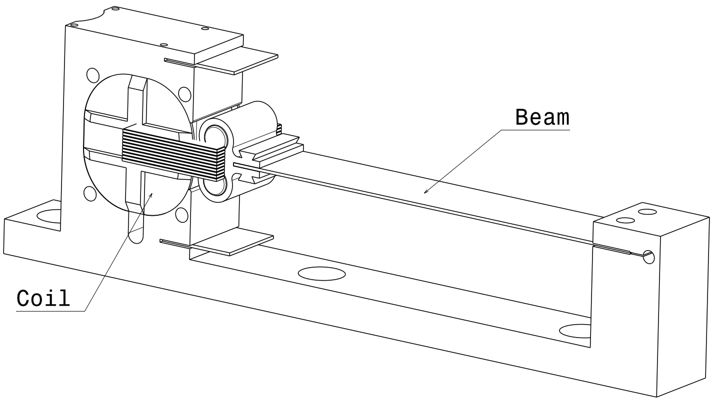

Figure 1.1: Schematic view of the prototype originally developed at SAAB.

The concept has been proved to work by creating a first prototype and testing it in a laboratory at Saab. At resonance (achieved at 29.7Hz) and acceleration level of 24.6 m/s^2 a power of 79.4 mW was produced. The complete results from this testing are found in Appendix B.

On behalf of Upwis AB, a wireless sensor technology company, Energy Harvesting Foundation has been asked to deliver a second version of the energy harvester. Their interest in the technology lies in the possibility of using it at railway cargo wagons for powering health monitoring systems. The prerequisite for continued partnership with Upwis is that Energy Harvesting Foundation delivers prototypes that align with a specification given, which basically requires scaling down the size of the device without significant loss in output power. The entire specification is found in Appendix C.

1.3 Purpose

The purpose of this thesis has been to assist Energy Harvesting Foundation with their product development for meeting the demands and completing the first prototype delivery to Upwis. Further, the purpose included to create a numerical model that can be used to predict and optimise the performance of the device for a variety of applications.

1.4 Scope

The thesis has comprised of three main areas

- Designing a prototype fulfilling the demand of Upwis
- Developing a numerical model for simulating the behaviour of the VEH technology
- Physical as well as virtual testing and verification of concepts

2

Vibration Energy Harvesting Using Electromagnetic Transduction

The following chapter will explain some of the fundamentals behind vibrations and how these can be converted into electricity through harvesting. It describes the theory of which the VEH is based and displays an analytical model that could be used to predict its behaviour. Further, it explain the physics behind the electromagnetic conversion and the limiting factors for energy harvesters using this mechanism.

2.1 Definition of vibration

As mentioned in the introduction, a mechanical system is vibrating when it is oscillating about an equilibrium position. All bodies with a mass and finite stiffness can vibrate and a common example to illustrate vibrations is the single degree of freedom (SDOF) mass-spring system shown in Figure 2.1 below.

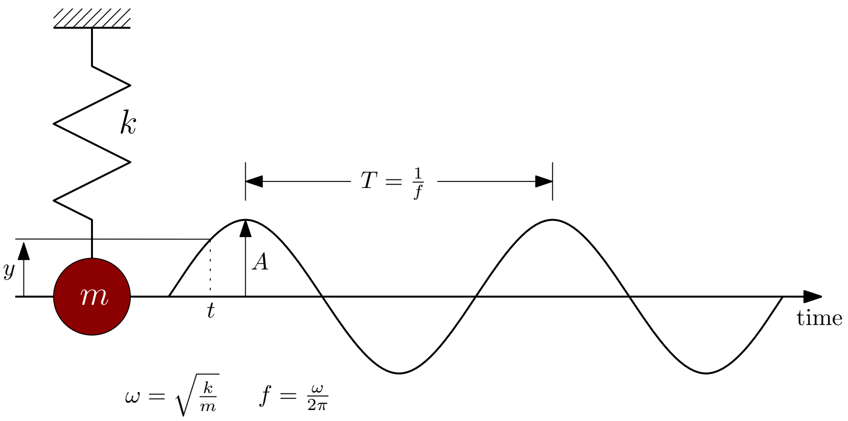

Figure 2.1: Illustration of SDOF system in free vibration where f is the vibration frequency, A is the vibration amplitude, T is the period time, and ω is the natural angular frequency.

In this example, the linear spring (symbolising the stiffness of the system) will always counteract the motion of the mass for returning it to its equilibrium position. The magnitude of the force of which the spring affects the mass is given by Hooke's law and hence is proportional to the displacement y from the equilibrium position. Mathematically, the simplest form of oscillation is harmonic and thus a way of describing the motion can be

$$y = A \sin \sqrt{\frac{k}{m}} t = A \sin \omega t \tag{2.1}$$

where A is the amplitude of the motion and ω is the natural angular frequency of the system. Taking the time derivative of the equation above provides an expression for the velocity of the harmonic motion

$$v = \omega A \cos \omega t \tag{2.2}$$

Judging from the equation above, the maximum velocity that can be achieved for this motion is ωA. The second time derivative will give the acceleration

$$a = -\omega^2 A \sin \omega t \tag{2.3}$$

2.2 Types and sources of vibration for harvesting applications

The sources of vibrations are various and we experience different examples of vibrations every day. Since vibrations can be very different in their characteristics depending on where they come from, all vibration sources may not be appropriate for energy harvesting applications. The following section will discuss different ways of categorising and considering vibrations in a VEH context and also present a survey on vibration data picked up from real-life applications.

2.2.1 Vibration characterisation

According to Schmitz and Smith [9], vibrations can be grouped into three main categories: free vibration, forced vibration, and self-excited vibration. In free vibration, a system is allowed to vibrate freely after being excited by some initial displacement, velocity or acceleration. When this happens the system will oscillate with its natural frequency until damping effects will stop the movement. This will be discussed further in *Section 2.3.1*, *Frequency tuning of resonant generators.* In forced vibration, some periodic excitation is applied to the system, which is the case for most vibration harvesting applications. If the excitation frequency is the same as the natural frequency of the system, resonance will occur and thus the maximum vibration amplitude is experienced. The last group is the self-excited vibration, or flutter. This occurs when an external steady force is "modulated into vibration near the system's natural frequency". In comparison to forced vibrations, the excitation force of self-excited vibrations is independent in a way that there is no physical coupling between the excitation source and the affected structure. A typical example of this is the wind affecting a building.

Another way to look at vibrations is to separate between periodic and random vibrations. The periodic vibration is typically the type that is generated by something that rotates. Let us say you are driving a car and notice that one of the disc brakes is squeaking when lightly hitting the brake pedal. As long as you drive with a constant speed, the noise will repeat with the same time interval. As mentioned earlier, the simplest periodic vibration is harmonic and can be described with functions such as the sine and the cosine. Random vibration is simply irregular in time and cannot be applied to any continuous function.

2.2.2 Level of vibration

Going back to the definition of vibrations and the harmonic function it is evident that vibration amplitude can be expressed in terms of acceleration. The SI unit for acceleration is m/s^2 but when it comes to vibrations it is often more convenient to express it in terms of the standard gravity constant g. A common acceleration measure is the g Peak-To-Peak (PTP), which reflects the total amplitude in the system and thus is appropriate to use when searching for total displacement or maximum energy of the vibration [10]. The Root-Mean-Square (RMS) is another measure that is common for describing the acceleration, which is a statistical average value reflecting the average energy of the vibration.

From Newton's II law of motion it is known that resulting force is equal to mass times acceleration and thus a higher level of acceleration implies greater forces. Having a look at Equation (2.3) one can see that the acceleration and thereby the force is proportional to the square of the angular frequency and needless to say the frequency of the vibration is also an important measure.

In a vibration energy harvesting context, low-frequency vibration can be defined as any vibration where the source motion amplitude is larger than the maximum internal displacement of the harvesting device [5]. This makes it complicated to design a VEH scavenging low-frequency vibrations and thus the efficiency of these harvesters is significantly lower than for those scavenging higher frequencies. *Section 2.4.1* will discuss more on how certain vibration levels are related to the power that can be generated through harvesting.

2.2.3 Presence of vibrations

Any structure in motion will generate a vibration signature that reflects its operating health [10]. In industry, this is a known fact and monitoring of vibrations in machines is common for maintaining optimum operating conditions but most importantly preventing failure and expensive downtime. For example, in rotating machinery vibrations will occur if all rotors are not perfectly aligned and turn true on their centreline. Since some level of imperfection or misalignment always will exist in a mechanical system, vibrations will exist too. This is why it is so important to keep track on machine health in industry. Of course not all kinds of vibrations are unwanted, there are devices designed to intentionally produce vibrations as well. However, those applications are probably not best benefiting from energy harvesting and thus are not the primary focus in this report.

In order to successfully design a vibration energy harvester one has to know the nature of vibration sources available. Roundy, Wright, and Rabaey [2] present a survey of different available vibration sources that is reproduced in Table 2.1. The measures are given in terms of frequency and acceleration magnitudes of the fundamental vibration mode, which refer to the frequency at which the acceleration is peaking. Judging from the content of the table one can draw the conclusion that the magnitude of each measure differs significantly between different vibration sources. However all the sources investigated by these authors can be classified as low-level vibrations that are not as energetic as those found in industrial applications.

Vibration source	a_{peak} [m/s^2]	f_{peak} [Hz]
Car engine compartment	12	200
Base of 3-axis machine tool	10	70
Blender casing	6.4	121
Clothes dryer	3.5	121
Person nervously tapping their heel	3	1
Car instrument panel	3	13
Door frame just after door closes	3	125
Small microwave oven	2.5	121
HVAC vents in office building	0.2-1.5	60
Windows next to a busy road	0.7	100
CD on notebook computer	0.6	75
Second store floor of busy office	0.2	100

Table 2.1: Vibration levels in various environments [2]

2.3 Linear resonators

Up to now, most energy harvesters based on converting vibrations are designed as linear resonators. This means the effective working frequencies of the VEH are close to the frequency at which the harvester resonates [11]. To express this differently, the resonance frequencies of the harvester have to be tuned based on the fundamental vibration frequency of the excitation source in order to achieve maximum power output.

2.3.1 Frequency tuning of resonant generators

To analytically find the exact solution for the natural frequencies of systems with distributed mass is complex and is only worked out for some certain shapes [8]. It is a fairly cumbersome and time-consuming process to work out the solution even for the most primitive geometries. Logically, continuously distributed parameter systems are in practice analysed using the Finite Element Method (FEM).

For a resonant generator based on a cantilever beam with a mass at the tip, there are basically three major ways to approach the modal analysis. If not using numerical tools such as FEM one can choose to use methods such as the Raleigh-Ritz for finding approximate resonant frequencies. An option to both these methods is to assume the mass of the beam to be much lighter than that for the tip mass. Hence, the system can be simplified and modelled as illustrated in Figure 2.2 below.

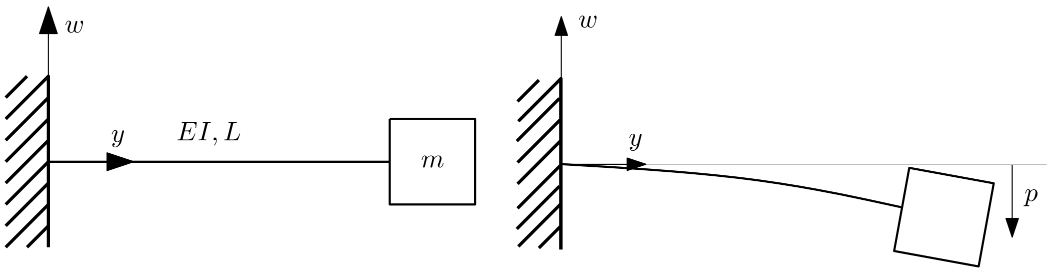

Figure 2.2: Cantilevered beam with tip mass much heavier than the beam itself

If neglecting the rotary inertia of the tip mass, this representation is actually no different to a free vibration single-degree mass system and therefore the equations of motion can be described as

$$m\ddot{x}(t) + \omega^2 x(t) = 0 \tag{2.4}$$

where ω is the undamped natural frequency. We know that

$$\omega = \sqrt{\frac{k}{m}} \tag{2.5}$$

and thus we are looking for an expression for the corresponding spring coefficient k.

TABULATED DEFLECTION CURVE: For an assumed Euler-Bernoulli cantilevered beam, a deflection p due to a tip force F is given as:

$$p = \frac{FL^3}{3EI} \tag{2.6}$$

where E is the Young's modulus, I is the moment of inertia, and L is the length of the beam. According to Hooke's law we have

$$k = \frac{F}{p} = \frac{3EI}{L^3} \tag{2.7}$$

If applying (2.7) to (2.5), the natural frequency f of the beam can be expressed as

$$\omega = \sqrt{\frac{3EI}{mL^3}} \Rightarrow f = \frac{\omega}{2\pi} = \frac{1}{2\pi}\sqrt{\frac{3EI}{mL^3}} \tag{2.8}$$

where m is the tip mass of the beam.

2.4 Discrete model of vibration converter

Once the system has been designed to resonate at the fundamental frequency of the host object it is desirable to create a more complete model to describe the harvester. Several authors [2], [12], and[13] have discussed the possibility of creating generic models of resonant generators by presenting them as spring-mass-damper systems with forced excitation. Figure 2.3 illustrates such a model, where y is the input displacement provided by the vibration source, x the motion of the mass, k the spring stiffness coefficient, and c the damping coefficient.

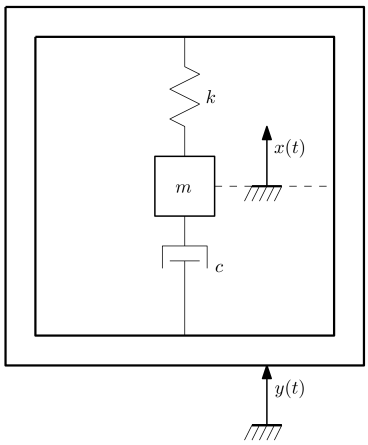

Figure 2.3: Illustration of single-degree mass-spring-damper with base excitation $y(t)$

NEWTON II:

$$-k((x(t) - y(t)) - c(\dot{x}(t) - \dot{y}(t)) = m\ddot{x}(t) \tag{2.9}$$

We denote the motion of the mass relative to the housing $z(t) = x(t) - y(t)$:

$$\begin{aligned} &-kz(t) - c\dot{z}(t) = m(\ddot{z}(t) + \ddot{y}(t)) \Rightarrow \\ &\ddot{z}(t) + \frac{c}{m}\dot{z}(t) + \frac{k}{m}z(t) = -\ddot{y}(t) \end{aligned} \tag{2.10}$$

Which in turn can be rewritten as

$$\ddot{z}(t) + 2\xi\omega\dot{z}(t) + \omega^2 z(t) = -\ddot{y}(t) \tag{2.11}$$

where ξ is the damping ratio and ω is the natural angular frequency of the vibration.

Assuming the excitation $y(t)$ to be harmonic with the form $y(t) = A\sin(\Omega t)$, the general solution to the equation is:

$$z(t) = \mathrm{e}^{-\xi\omega t}[C_1 \sin\omega_\mathrm{d} t + C_2\cos\omega_\mathrm{d} t] - \lambda\frac{A\Omega^2}{\omega^2}\sin(\Omega t - \psi) \tag{2.12}$$

Here

$$\tan\psi = \frac{2\xi\Omega\omega}{\omega^2 - \Omega^2} \tag{2.13}$$

$$\lambda = \frac{\omega^2}{\sqrt{(\omega^2-\Omega^2)^2 + 4\xi^2\Omega^2\omega^2}} \tag{2.14}$$

$$\omega_\mathrm{d} = \omega\sqrt{1-\xi^2} \tag{2.15}$$

Initial Conditions:

$$\tag{2.16}$$

Starting from rest, we have that

$$z(0) = 0 \Rightarrow C_2 = -\lambda\frac{A\Omega^2}{\omega^2}\sin\psi \tag{2.17}$$

$$\dot{z}(0) = 0 \Rightarrow C_1\omega_\mathrm{d} - C_2\xi\omega - \lambda\frac{A\Omega^3}{\omega^2}\cos\psi = 0 \tag{2.18}$$

Adding (2.16) to (2.17) gives

$$\begin{aligned} &C_1\omega_\mathrm{d} + \xi\omega\lambda\frac{A\Omega^2}{\omega^2}\sin\psi - \lambda\frac{A\Omega^3}{\omega^2}\cos\psi = 0 \Rightarrow \\ &C_1 = \frac{\lambda A\Omega^3}{\omega_\mathrm{d}\omega^2}\cos\psi - \frac{\xi\omega\lambda A\Omega^2}{\omega_\mathrm{d}\omega^2}\sin\psi = \frac{\lambda A\Omega^2}{\omega_\mathrm{d}\omega^2}(\Omega\cos\psi - \xi\omega\sin\psi) \end{aligned} \tag{2.19}$$

Thus

$$z(t) = \mathrm{e}^{-\xi\omega t}C[\frac{1}{\omega_\mathrm{d}}\sin\omega_\mathrm{d} t(\Omega\cos\psi - \xi\omega\sin\psi) - \cos\omega_\mathrm{d} t\sin\psi] - C\sin(\Omega t - \psi) \tag{2.20}$$

where

$$C = \frac{\lambda A\Omega^2}{\omega^2} \tag{2.21}$$

As it shows, we are left with an expression that describes the relative displacement $z(t)$. Adding (2.13), (2.14) & (2.15) to Equation (2.19) will show that the only unknown factor is the damping coefficient ξ. Recalling that $\frac{c}{m} = 2\xi\omega$ gives $\xi = \frac{c}{2m\omega}$.

2.4.1 Damping and power estimation

All vibrating systems are subject to some form of damping or energy dissipation. If there would be no losses in the form of damping the free vibration of a seismic mass would theoretically continue with the same amplitude indefinitely. Since this does not happen in real life applications, some sort of damping has to exist. In a vibration energy-harvesting context the damping of the system can be divided into two major categories: parasitic mechanical losses and energy converted into electricity through the transduction mechanism [12]. Hence, the expression for the equivalent damping ξ is

$$\xi = \xi_{\text{mechanical}} + \xi_{\text{electrical}} \tag{2.22}$$

So, the power that can be extracted from a vibratory system is related to the energy that can be dissipated through damping [4]. The instantaneous power transfer $p(t)$ is the product of the force acting on the mass and its velocity, expressed as

$$p(t) = -m\ddot{y}(t)[\dot{y}(t) + \dot{z}(t)] \tag{2.23}$$

When considering the effect of damping due to the electromagnetic transduction, there is a net transfer of mechanical power into electrical power. For a sinusoidal ambient vibration source, $y(t) = A\cos\Omega t$, Equation (2.21) can be adjusted to express the average electric power generated

$$P_{\text{average}} = \frac{m\xi A^2(\frac{\Omega}{\omega})^3\Omega^3}{[1-(\frac{\Omega}{\omega})^2]^2 + [2\xi\frac{\Omega}{\omega}]^2} \tag{2.24}$$

This way of expressing the power output of a vibration energy harvester was first presented by Williams and Yates [12]. Assuming that the excitation frequency is equal to the resonant frequency of the system ($\omega = \Omega$), the equation will reduce to

$$P_{\text{average}} = \frac{mA^2\Omega^3}{4\xi} \tag{2.25}$$

If considering the mass-and-spring representation of the vibrating system mentioned earlier it is straightforward to see that vibrations can be thought of as a continuous alternation between kinetic energy of the moving mass and potential energy stored in the spring. For the same amplitude, a higher frequency vibration will provide more kinetic energy (higher speed) than a low frequency. This relation is also shown in the equation above, where the average power is proportional to the cube of the vibration frequency.

2.4.2 Bandwidth

The bandwidth of a linear resonator is limited since the span of productive operation frequencies is narrow. In case of having an unknown or varying excitation source, a narrow-band linear resonator might not be the optimum choice in order to secure a reliable power supply. In such a situation it is often desirable to make the harvester respond to a wider range of frequencies or simply make it adapt to the changing conditions. The different approaches for broadband energy harvesters are many and Twiefel and Westermann [7] suggest a way of how some of these can be grouped by different categories of conversion techniques: linear generators, nonlinear generators, and advanced electronic networks (see Figure 2.4).

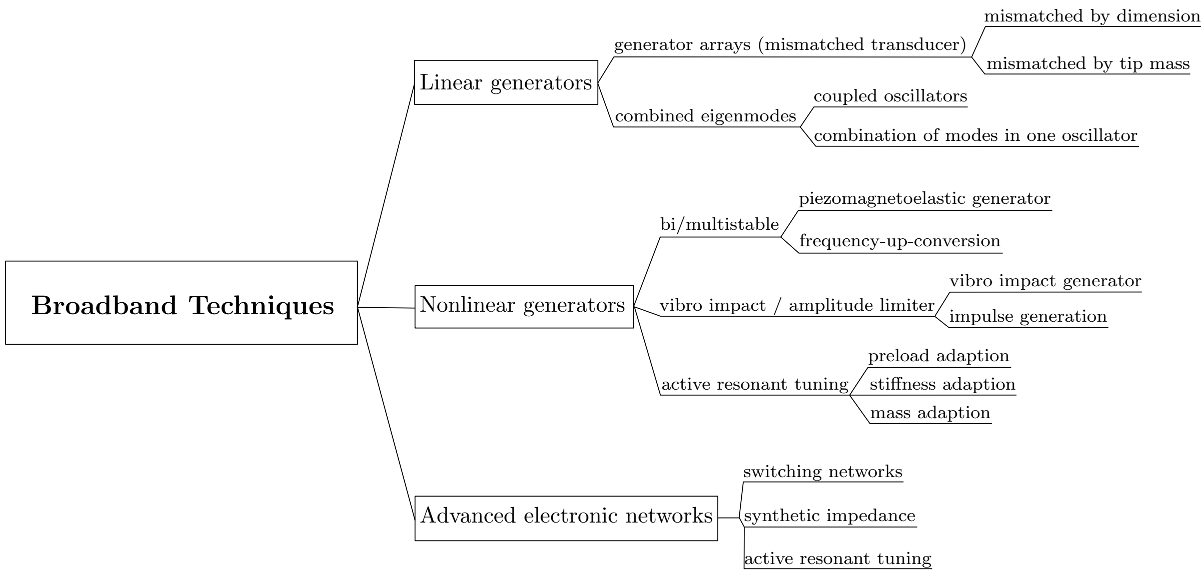

Figure 2.4: Different techniques for broadening the bandwidth of a VEH [7]

The first two categories have somewhat been introduced already but the latter is referring to the fact that advanced electronics can be used in parallel with i.e. a piezoelectric elements in order to improve the power generation. In other words, it refers to modifying the electrical load to increase the performance of the VEH.

For linear resonators, Twiefel and Westermann [7] introduced "generator arrays" as one way of increasing the bandwidth. As it sounds, this refers to using multiple cantilevers having different resonance frequencies. This is in turn achieved by either tuning the geometry (dimensions) of the beam as illustrated in Figure 2.5(b) below or by adding/subtracting mass from the tip of the beam. For advantages and disadvantages together with suitability for each broadband approach introduced by these authors it is referred to the specific article [7].

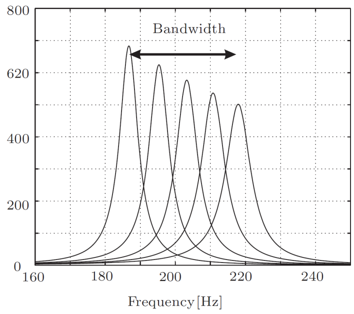

(a) The productive range of frequencies increases with an array.

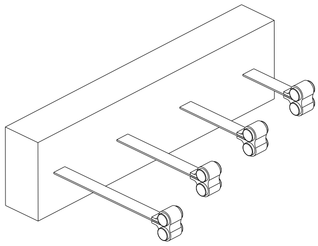

(b) Schematic of harvester array with different beam length.

Figure 2.5: Illustration of the increased bandwidth by using an array of harvesters [7].

2.5 Electromagnetic Conversion

As described in *Section 2.4.1* an "electrical damping mechanism" exist in all vibration energy harvesting devices when energy is converted from mechanical movement to electricity. The efficiency of this electromagnetic conversion determines how much power that can be generated. The following sections describe the fundamental theory behind this transduction mechanism and briefly cover the two most important types of energy loss in this process.

2.5.1 Magnetic Fields

Magnetic fields can be found around permanent magnets and around conductors that carry current. In both cases, the source of the magnetic field is electrical charge in motion [14]. The magnetic flux, denoted Φ, determines the strength of the magnetic field through the surface area A according to

$$\Phi = \int_A B \mathrm{d}A \tag{2.26}$$

where B is the magnetic flux density. If the the magnetic flux density is constant and perpendicular to the surface, Equation (2.26) can be reduced to

$$\Phi = BA \tag{2.27}$$

In 1831, Michael Faraday discovered that a current was induced in a loop of copper-wire when the magnetic flux in the loop changed [15]. This phenomena, nowadays known as Faraday's law of electromagnetic induction, states that the induced voltage in a stationary closed circuit is equal to the negative rate of change of the magnetic flux linking the circuit

$$U = -\frac{d\Phi}{dt} \tag{2.28}$$

If assuming that the same flux surround each turn of the coil, which is often a good approximation [14], the induced voltage U in the coil is

$$U = -N\frac{d\Phi}{dt} \tag{2.29}$$

where N is the number of loops in the coil. The magnetic flux density is highly dependent on which material the magnetic field is applied on and this relationship is described by the magnetic field intensity H. The relationship between magnetic flux density B and magnetic field intensity is given by

$$B = \mu H \tag{2.30}$$

where μ is the permeability of the material describing the ability for a material to support the formation of a magnetic field within itself. For free space the permeability is

$$\mu_0 = 4\pi \cdot 10^{-7}\mathrm{Wb/Am} \tag{2.31}$$

The presence of a magnetic material will enhance the magnetic flux density and often the permeability of a material is given as a relation to the permeability of free space such as

$$\mu_r = \frac{\mu_{\mathrm{material}}}{\mu_0} \tag{2.32}$$

Equation (2.30) can thus be rewritten as

$$B = \mu_0\mu_r H \tag{2.33}$$

According to Ampere's circuital law the line integral of the magnetic field intensity around a closed path is equal to the sum of the free current flowing through the surface bounded by path C [15]. This law is formulated as

$$\oint_C H\mathrm{d}l = I \tag{2.34}$$

In which $\mathrm{d}l$ is a vector element of the length with direction tangent to the path of integration.

2.5.2 Magnetic Circuits

The magnetic flux and magnetic fields are often analysed using magnetic circuit analysis. From Ampere's circuital law the magnetomotive force F_{mmf} on a current carrying coil with N turns enclosing the path C is

$$\oint_C H\mathrm{d}l = Ni = F_{\mathrm{mmf}} \tag{2.35}$$

When a magnetic field is propagating in a material there is always some form of resistance. In magnetic field theory this resistance is denoted reluctance and is given by

$$\mathcal{R} = \frac{l}{\mu A} \tag{2.36}$$

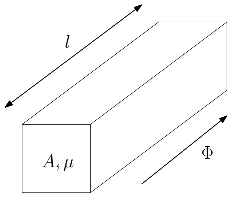

When the magnetic field Φ passes through a material with cross-sectional area A, length l and permeability μ the reluctance, magnetomotive force and magnet flux is related by

$$F_{\text{mmf}} = \mathcal{R}\Phi \tag{2.37}$$

2.5.2.1 Magnetic Circuit of the VEH

From Faraday's law it is known that the magnitude of the induced voltage depend on the rate of change of the magnetic flux, which in turn depend on the magnitude of the magnetic flux and the frequency of the shifting direction of the magnetic field. It is therefore desirable to maximise the magnetic flux in the magnetic circuit. When the direction the magnetic flux switches there will be some dynamic effects in the core. These dynamic effects will be discussed in *Section 2.5.3*. Concerning the strength of the magnetic flux in the VEH's magnetic circuit this could be analysed in a stationary mode where the stationary magnetic field of the VEH can be represented by Figure 2.6

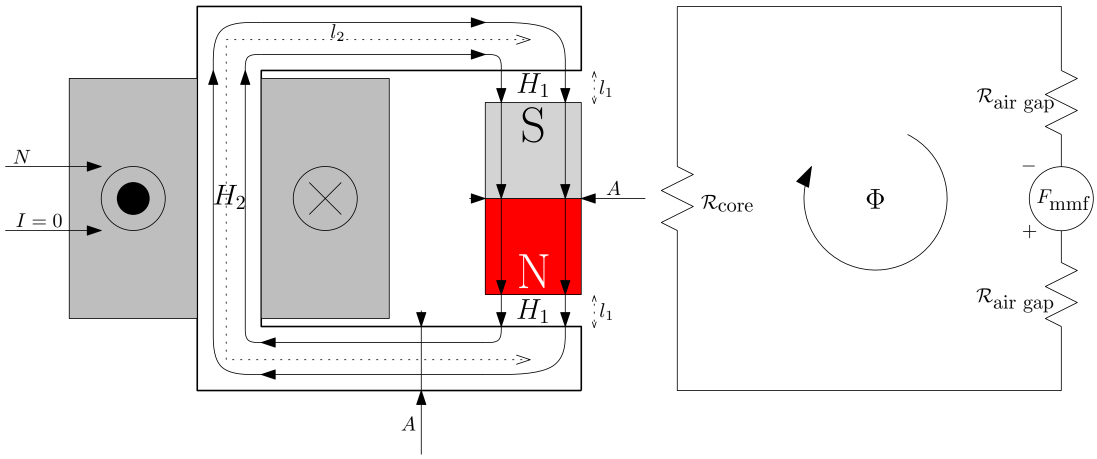

Figure 2.6: Magnetic circuit of the VEH where H_1 is the magnetic field intensity in the air gaps and H_2 is the magnetic field intensity in the core. The reluctances in the air gaps and core are illustrated on the right side of the illustration.

From Ampere's law the following relationship is obtained for the magnetic circuit

$$2H_1 l_1 + H_2 l_2 = F_{\text{mmf}} \tag{2.38}$$

where H_1 is the magnetic field intensity in the air gaps, l_1 is the length of the air gap, H_2 is the magnetic field intensity in the core, and l_2 is the length of the core.

By using equation (2.27), (2.33) and (2.37) this can be rewritten as

$$H_i l_i = \mu_0 \mu_i H_i A_i \frac{l_i}{\mu_0 \mu_i A_i} = \Phi_i \mathcal{R}_i \tag{2.39}$$

where i = 1,2,3,...

The strength of the magnetic flux Φ passing the magnetic circuit of the VEH will depend on the strength of the permanent magnet creating the magnetic field and the total reluctance in the circuit. With the assumption that $\Phi_1 = \Phi_2 = \Phi$ the following relationship is obtained

$$\Phi = \frac{1}{2\mathcal{R}_1 + \mathcal{R}_2} F_{\mathrm{mmf}} \tag{2.40}$$

Equation (2.36) shows that the reluctance $\mathcal{R}$ is highly dependent on the permeability μ of the material. As mumetal has a relative permeability μ_r of 20000 [16], the following relationship of the total reluctance in the circuit exists

$$\mathcal{R}_{\mathrm{tot}} = \frac{2l_1}{\mu_0 A} + \frac{l_2}{20000\mu_0 A} = \frac{1}{\mu_0 A}(2l_1 + \frac{l_2}{20000}) \tag{2.41}$$

The above relationship clearly shows that the length of the airgap l_1 has much more impact on the total reluctance than the length of the core l_2. For example, if the airgap is 1 mm the length of the core would have to be 40 m in order to affect the total reluctance as much as the airgap. So, to maximise the magnetic flux Φ in the magnetic circuit, the length of the airgap l_1 should be minimised.

2.5.3 Magnetic Materials

When dealing with electromagnetic transduction there will always be some form of energy loss. The transduction mechanism used in the VEH is very similar to that of a transformer which operate under a.c conditions [17]. The two main sources of loss in transformer cores are hysteresis and eddy current loss. Both hysteresis and eddy current loss are highly dependent on on the frequency and magnitude of the applied magnetic field. To minimise these losses it is vital to use the most appropriate materials for the application at hand.

2.5.3.1 Hysteresis loss

The $B - H$ curve in Figure 2.7 represents the behaviour of magnetic materials when a cyclic field intensity H is applied. This curve is commonly known as a hysteresis loop and the shaded area within it illustrates the energy loss per cycle, denoted hysteresis loss [18].

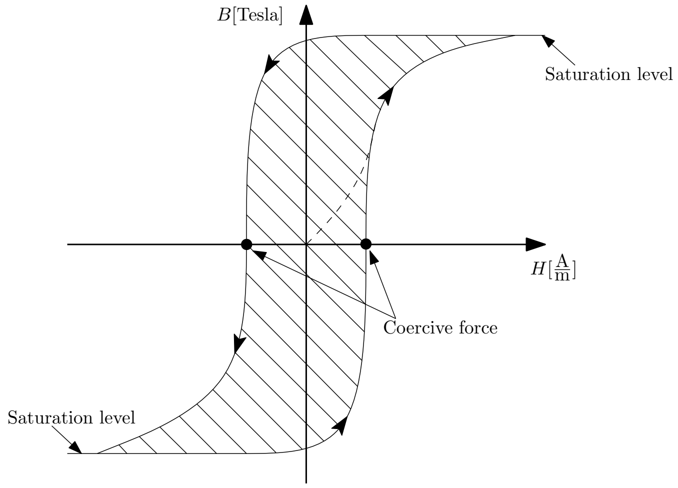

Figure 2.7: Hysteresis loop of a magnetic material

The magnetising field H required to demagnetise a material is called the *coercive force* and symbolises the material's resistance to demagnetisation. Based on their B-H behaviour, magnetic materials are often classified into soft and hard magnetic materials. Soft magnetic materials have a low coercivity and thus require a low coercive force in order to magnetise or demagnetise, resulting in a very narrow hysteresis loop and low hysteresis losses. These materials are typically used in generator and transformer cores. Hard magnetic materials, such as permanent magnets, have high coercivity and are only demagnetised if affected by a very high magnetic field.

2.5.3.2 Eddy Current loss

The magnetic materials used in cores are in many cases iron-based and thus are good conductors. When a time-varying magnetic field acts on a conductive material a voltage will be induced that in turn will drive currents within the material. These currents are called eddy currents and will dissipate as heat within the core [18], see Figure 2.8(a). One way to reduce these eddy current losses is to split the core into many small cores through lamination. By electrically insulating these laminates from each other the conductivity of the core will be drastically reduced and hence the eddy current loss is reduced too (see Figure 2.8(b)).

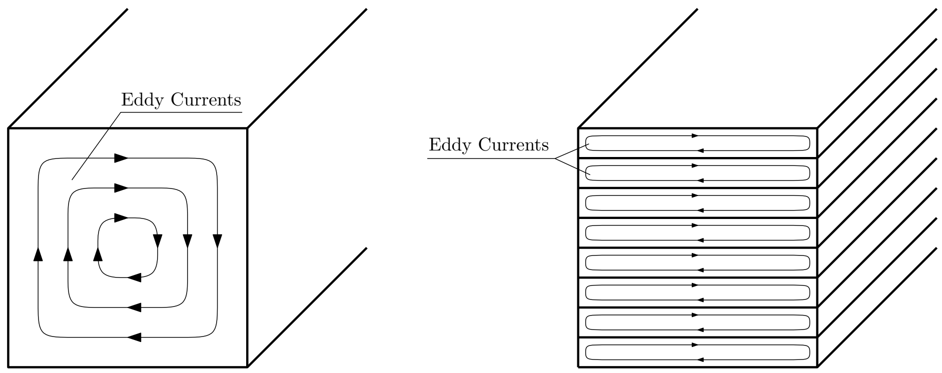

(a) Eddy currents in a solid core.

(b) Eddy currents in a laminated core.

Figure 2.8: Illustration of the eddy currents in a magnetic core exposed to a time-varying magnetic field. [7]

The drawback with using too thin laminates is that the total amount of magnetic material in the core will be reduced due to the added insulation material. This will in turn reduce the permeability of the core and hence the strength of the magnetic field passing through it. Since the the eddy current loss is highly dependent on the frequency of the varying magnetic field, the sheet thickness is a clear trade-off design parameter between the permeability of the core and the power loss due to eddy currents.

3

Prototype Development

The first part of the project was directed towards meeting the customer requirements with a particular focus of testing the improved VEH in a real-life application by the end of March. This section will guide you through the process of how the customer specification converted into empirical test results and how those came to affect the design of the second generation prototype.

3.1 Defining subsystems

The project started out at a point where neither of the authors of this report had a particularly good understanding of the functionality of the harvesting technology. So, in order to improve its design a greater level of understanding about the technology had first to be acquired. A natural way of breaking down the problem into pieces was categorising the structure of the VEH by two separate subsystems: the mechanical subsystem and the electromagnetic subsystem. The former consisting of the oscillating spring together with its tip mass (mass of holder and magnets), see Figure 3.1(a). The latter constituting the magnetic circuit with the copper coil, the magnets, and the mumetal core, Figure 3.1(b). By studying these two subsystems, key parameters could be identified and further analysed through testing.

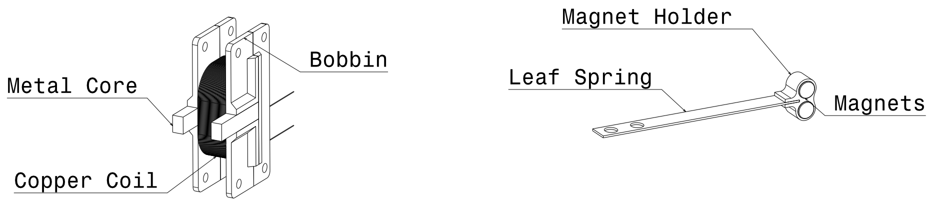

(a) Mechanical subsystem

(b) Electromagnetic subsystem

Figure 3.1: Illustration of the two subsystems constituting the base technology of the VEH

3.1.1 Mechanical subsystem

The mechanical subsystem is the heart of the harvester that provides the changing magnetic field needed for a current to be induced in the coil. At rest, the magnets are placed in the middle of the mumetal column as shown in Figure 3.2(a). When the spring is deflected upwards the magnetic field will take one direction according to Figure 3.2(b). Thanks to having the two magnets mounted with reversed polarity, the direction of the magnetic field will change when the spring is later deflected downwards as shown in Figure 3.2(c).

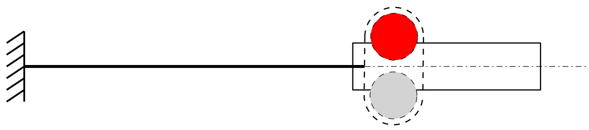

(a) At rest, the spring is pointing directly towards the magnetic core

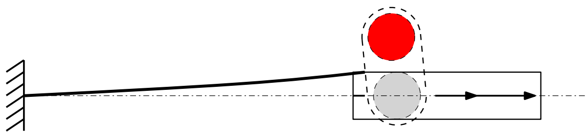

(b) When the spring is deflected upwards, the lower magnet is affecting the core alone

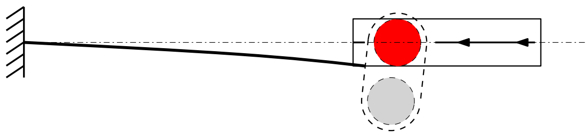

(c) The direction of the magnetic field changes with the direction of the spring

Figure 3.2: Illustration of how the movement of the spring change the direction of the magnetic field

The amplitude by which the spring-mass system oscillates when making it subject to vibrations is a direct function of its mechanical properties as well as the amplitude and frequency of the surrounding vibrations (see *Section 2.2*). In order to provide the deflection needed for the magnetic field to change, the excitation frequency usually has to lie near the natural frequency of the mechanical subsystem. This will cause the latter to resonate and thus maximum amplitude will be experienced in the spring. In this case, 60Hz was stated to be the driving frequency and thus a design requirement from the customer (see Appendix C).

As mentioned in *Section 2.4.2*, adjusting the natural frequency of the mechanical subsystem can be done by either adding or subtracting to the tip mass or simply adjusting the mechanical properties of the spring. This means that the variables affecting the modal behaviour are:

- Length, width, and thickness of spring
- Material of spring (Young's modulus)
- Weight of magnets
- Weight of magnet holder

In addition to the above, a too large deflection of the spring can become critical in terms of fatigue. Figure 3.3 illustrates how a subsystem with small magnets (a) requires a rather short distance of travel w_2 to make a clear change of field polarity compared to the case of having larger magnets in case (b), where p_1 is about twice the distance of p_2.

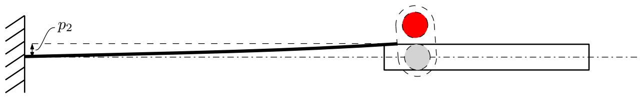

(a) Required deflection when using small magnets

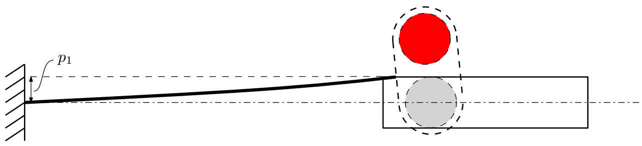

(b) Required deflection for large magnets

Figure 3.3: Schematic on how different sizes on magnets affect the required deflection of the spring

3.1.2 Electromagnetic subsystem

As mentioned earlier, the electromagnetic subsystem consists of the three main components magnets, core, and coil. In Figure 3.4 below it is illustrated how this subsystem also can be considered a magnetic circuit.

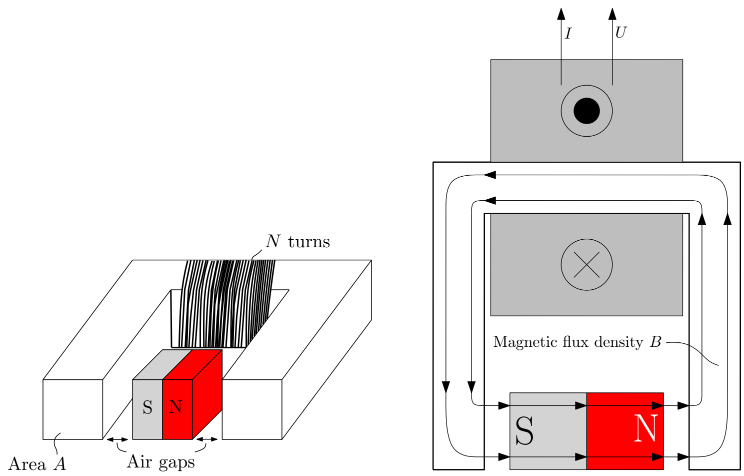

(a) The coil consists of a number of wire windings around the core

(b) Magnetic circuit with flux lines going through the coil

Figure 3.4: Illustration of how the electromagnetic subsystem make up a magnetic circuit

With the aim to maximise the power output of the VEH the different components in the electromagnetic subsystem where analysed. As described in *Section 2.5.1*, the magnitude of the magnetic flux Φ passing through the coil should be maximised in order to maximise the induced voltage in the coil. This is stated by Faraday's law of electromagnetic induction

$$V = -N\frac{d\Phi}{dt} = -N\frac{dAB}{dt} \tag{3.1}$$

According to the equation above, the magnetic flux is equal to the magnetic flux intensity B times the cross-sectional area A perpendicular to the magnetic field. In other words, the cross-sectional area of the core will also have an impact on the strength of the magnetic flux.

Regarding the permanent magnets, the primary factor of importance for maximising the magnetic flux Φ is the magnetic strength these can provide, which in turn depend on the material of the magnet used as well as its volume. The magnetic flux that can be transferred to the magnetic core also depends on the length of the air gap between magnets and core, which was explained in *Section 2.5.2.1*. Thus, the magnetic strength of the magnets and the length of the air gap will be important factors determining the strength of the magnetic flux passing through the core.

When designing the core the permeability and the core loss are the two most important factors to consider. As described in *Section 2.5.3* hysteresis and eddy current losses will arise when a cyclic magnetic field is applied to the core. In order to ensure small hysteresis loss and high permeability it is vital to chose the right core material. Constructing the core from a bundle of thin laminates being electrically insulated from each other, eddy current losses will be lower than for the case of using a solid core. Decreasing the thickness of the laminates will reduce the eddy current losses but also the permeability of the core.

Regardning the coil, two major parameters were identified to have an impact on the performance, namely the number of turns and the wire diameter. According to Faraday's law above, the induced voltage is proportional to the number of turns N of the coil. The wire diameter on the other hand, affects the number of turns possible to place within a certain volume as well as the resistance of the coil - which in turn will determine how much current that will pass through it.

3.2 Finding power-determining parameters

The identified parameters that in some way would have an impact on the power generated by the VEH are listed in Table 3.1. In order to identify how these parameters affected each other and thus finding the way of maximising the power output, the Design of Experiments (DOE) methodology was applied.

Table 3.1: Identified parameters determining the performance of the VEH

Factor	Type of Impact
Mechanical subsystem	
A: Beam dimensions	Affects deflection and modal behaviour
B: Beam material	Affects deflection and modal behaviour
C: Magnet holder dimensions	Affects deflection and modal behaviour
D: Magnet holder material	Affects deflection and modal behaviour
E: Magnet dimensions	Affects deflection and modal behaviour
F: Magnet material	Affects deflection and modal behaviour
Electromagnetic subsystem	
G: Number of coil windings	Affects level of induced voltage
H: Coil wire diameter	Affects number of turns and resistance
I: Coil material	Affects conductivity
J: Magnet strength	Affects magnetic field strength
K: Core dimensions	Affects magnetic field strength
L: Core material	Affects coercivity and conductivity
M: Core lamination thickness	Affects eddy currents and permeability
N: Air gap	Affects magnetic field strength

With DOE terminology, the parameters being subject for the study are referred to as the *factors* [19]. The *sample size*, i.e. the number of runs needed to perform the test increases with added number of factors. An important thing to determine is the different values or categories each factor can assume and should be tested at. These are called the *levels* and are typically given a high and a low value. In this case, the the goal was to meet the demands of the customer in terms of power output but also the size of the device. For example, this lead to the fact that large magnets were desirable for their strength but they could not be so large that they would make the overall design exceed its maximum size.

If a difference in response between the levels of one factor is not the same at all levels of the other factors, there is an *interaction* between the factors. According to [19], a “significant interaction will often mask the significance of main effects”. This means that in presence of noteworthy interactions it is more convenient to know about these rather than the effect of single factors. Starting from an assumption that noteworthy interaction existed, a full factorial design was used in order to avoid any misleading conclusions. That is a DOE approach implying that all possible combinations of factor levels are investigated during the experiment.

The sample size needed to conduct a full factorial design with two levels is given as

$$N = 2^F \tag{3.2}$$

where F is the number of factors. In other words, testing all of the identified parameters would require as many as $2^{14} = 16384$ runs. Clearly, this would have become far too costly and cumbersome to conduct in a real test and therefore it was necessary to find a way of reducing the number of factors.

3.2.1 Screening of identified parameters

To start with, all parameters were not equally interesting to evaluate. For example, there were no reason to test other coil materials than what is usually used in this kind of applications, namely copper. All other materials used in the set-up were chosen based on the same argument and thus factor B, D, F, I, and M were held constant during the test.

At this stage the most vital function of the mechanical subsystem was its modal behaviour and its required deflection. As this could be analysed with high precision using FE simulations in Ansys® (see *Section 3.3.1*) there was no need to include these parameters in the physical tests. Consequently, factors A-F also fell out of the testing space.

The magnet strength, air gap and lamination thickness will determine the strength of the magnetic field passing through the coil and thus are all very important performance parameters. Regarding the air gap (*Factor N*), this should be as small as possible in order to minimise losses and was thereby not considered important to evaluate at this stage. In other words, it was minimised and thereby the magnet strength *Factor J* and the lamination thickness *Factor M* became the main factors determining the magnetic field strength and thus were added to the tests.

The number of windings in the coil will, according to Faraday's law, proportionally determine the induced voltage in the coil. The wire diameter will in turn affect amperage. Since there was a physical limit regarding the overall size of the coil it was evident that the number of wire windings also was limited. Due to the fact that there was no obvious reason not to fill the coil space entirely it was decided to maximise the windings and instead evaluate the effect of varying the wire diameter.

Due to the structure of the technology, some parameters were automatically linked and hence varying one would automatically vary the other. This kind of dependency exists between the magnet diameter and the core height as the magnet need to fit the core, see Figure 3.2. To decouple the the magnet size (magnet strength) from the core height it was decided to vary the length of magnet rather than the diameter in order to vary the magnetic strength of the magnet.

Finally, it all came down to the three remaining factors *Magnet length*, *Coil diameter*, and *Lamination thickness*. The next thing to do was identifying appropriate levels at which these factors should be tested. The length of the magnets was easy to decide since these were directly related to the width of the VEH, which in turn was constrained by the customer. The other two factors required a bit more investigation before the levels were finally set within a range based on what is used in similar applications, e.g. transformers etc. The test factors with levels are presented in Table 3.2.

Table 3.2: Final test factors with corresponding levels

Factor	Low level (-1)	High level (1)
A: Magnet length	8 mm	10 mm
B: Coil wire diameter	0,2 mm	0,4 mm
C: Core lamination thickness	0,2 mm	0,4 mm

Table 3.3: DOE Design Matrix

		Factors						
Experiment nr.	Run nr.	A	B	C	AB	AC	BC	ABC
1	5	-1	-1	-1	1	1	1	-1
2	2	1	-1	-1	-1	-1	1	1
3	7	-1	1	-1	-1	1	-1	1
4	6	1	1	-1	1	-1	-1	-1
5	1	-1	-1	1	1	1	1	1
6	3	1	-1	1	-1	-1	1	-1
7	8	-1	1	1	-1	1	-1	-1
8	4	1	1	1	1	-1	-1	1

According to the DOE methodology [19], a design matrix was constructed and can be found in table 3.3. Here, -1 represents low level and 1 stands for high level. In order to reduce noise the run order was randomised.

3.3 Preparation of test

The check-list to go through before any test could be carried out was long and most of all challenging to complete in time. First of all, some kind of shaking device was needed on which to mount the VEH during the actual testing day. Most importantly however, the different test parameters had to be incorporated into the design in some easy and smart way. In this case, creating a virtual model of the prototype using CAD made it possible to easy define the interfaces of the different parts and thereby functionality could be assured.

3.3.1 Design of mechanical subsystem

One of the many decisions that had to be made was choosing an appropriate spring material. Finally, it all came down to what could be procured in time and the steel alloy 1770-04 was selected. This is a standard spring material with Young's modulus of 208,5 GPa used in a great variety of products [20]. The springs needed for the test were provided by Lesjöfors as a free sample, readily cut into desired widths.

As mentioned earlier, the mechanical subsystem had some limitations regarding its overall measurements due to the customer specification. On the other hand, these were not too many and there were still many variables that could be adjusted freely in order to meet the goal of having the spring-mass system resonating at a particular frequency.

This resulted in an iterative design process where spring and magnet holder properties were varied.

In order to tune the properties of the mechanical subsystem in way that would make it resonate at 60Hz, a FE model was created using Ansys. By utilising the module for modal analysis, the natural frequencies of the system could be obtained fast and easy (Figure 3.5). Particularly, using this method was faster and in particular more accurate than analytically calculating the frequency since the entire subsystem could be analysed at once without making approximations. It is to be noted that only the first eigenmode was of interest for this analysis and thus tuning solely covered this mode.

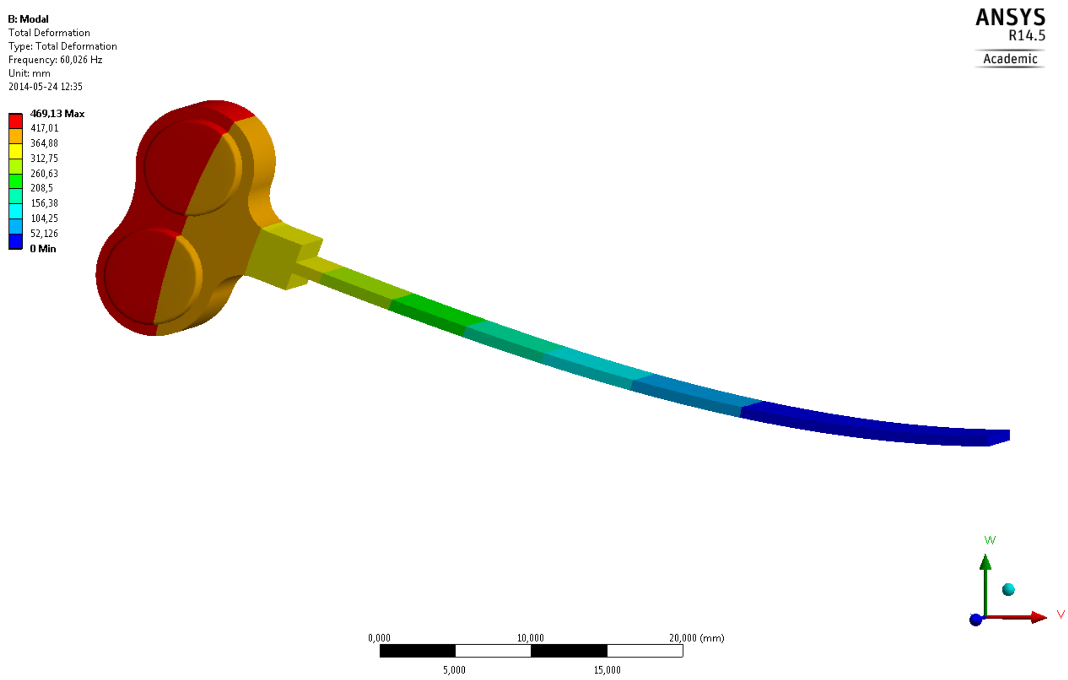

Figure 3.5: Screen dump from Ansys modal analysis showing the shape of the first resonance mode. Here the system resonates at 60.026Hz

The properties of the mechanical subsystem providing the system to resonate at 60.026Hz were compared to Equation (2.8) expressed in *Section 2.3* as

$$f = \frac{1}{2\pi}\sqrt{\frac{3EI}{mL^3}} = 60.8\text{Hz} \tag{3.3}$$

In conclusion, the simplified analytical solution differed slightly from the FE dito.

3.3.2 Design of electromagnetic subsystem

For the test, eight different electromagnetic subsystems were created. It was key making those right from the beginning and therefore a lot of effort was put into creating a good and robust design.

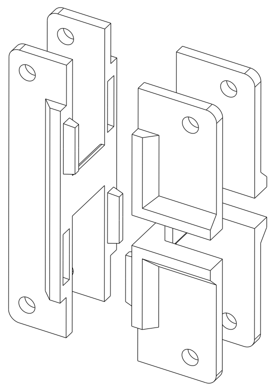

Figure 3.6: Two-part bobbin design

In order to avoid damaging the coil by winding it directly onto the sharp-edged core, a bobbin was designed. This was created in two parts in order to make manufacturing possible (see Figure 3.6). The main challenge in designing the bobbin was to minimise wall thickness (insulation) between the core and the coil but still achieving satisfying robustness. Some features that were added to the bobbin are:

- Small guide pins to facilitate aligning the two half's when assembled.
- Supports for the mumetal for avoiding movement.
- A design for maximised coil space.
- A design for easy installation.

In order to allow the spring to oscillate freely and thus assure functionality of the prototype it was crucial to design the mumetal core with a large enough air gap according to Figure 3.4(a). Different designs were tested before a clearance of 0.3 mm on each side was set.

3.3.3 Modular test fixture

To effectively perform the tests with minimised noise and error sources, two different fixtures were developed and produced. These were primarily designed to fit the different magnet lengths to be tested and therefore only varied in how wide they were. By creating a modular design on the fixtures as well as standardising the bobbin design, the entire range of coil designs could be tested using only two fixtures.

Figure 3.7 illustrates the design of the rig. Apart from the two subsystems it consists of four main parts: a bottom rail with a longitudinal groove (1), a bobbin housing (2), an adjustable spring attachment (3), and brackets for limiting the maximum spring deflection (13). Notice that it was only part (2) that differed between the two rigs.

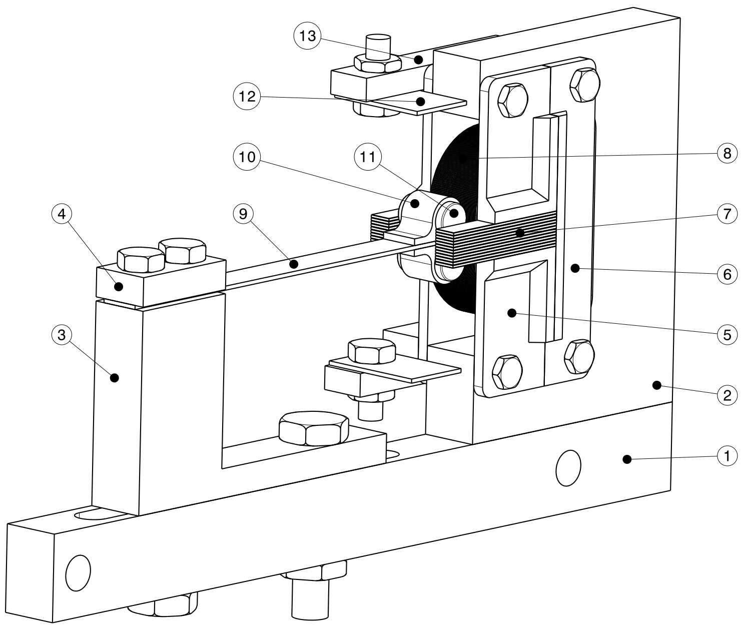

Figure 3.7: The modular test rig

The modular testing gear minimised the number of parts needed to be manufactured and thereby variance in production became less important as well as the availability of machines in the workshop became less limiting. For a complete description of the parts, see Table 3.4.

Table 3.4: Bill-of-material of the test rig.

Nr	Item	Material
1	Base fixture	EN7075
2	House fixture	EN7075
3	Holder fixture	EN7075
4	Top block	EN7075
5	Bobbinhalf 1	Thermosetting plastic
6	Bobbinhalf 2	Thermosetting plastic
7	Magnetic core	Mumetal
8	Coil	Copper
9	Beam	SS1770-04
10	Magnet holder	EN7075
11	Magnet	NdFeB
12	Amplitude limiter	SS1770-04
13	Amplitude limiter holder	EN7075

3.4 Manufacturing and purchase of test equipment

The two test rigs were entirely manufactured in wrought aluminium alloy 7075 (see Figure 3.8). This is a high-strength material with good manufacturability and hence appropriate for fast production. All parts but the magnet holders were manually machined using the mills available at Chalmers.

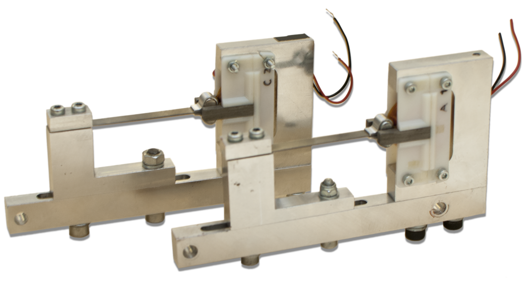

Figure 3.8: The milled test fixtures

The mumetal core was produced by stacking a series of thin plates on top of each other. These were produced by a manufacturer using photo etching, a manufacturing method providing the fine tolerances needed to ensure the clearance between the magnets and the core. Before assembling the cores using custom made stacking fixtures (see Figure 3.9(a)) and glue, the sheets were sprayed with varnish for insulating them from each other.

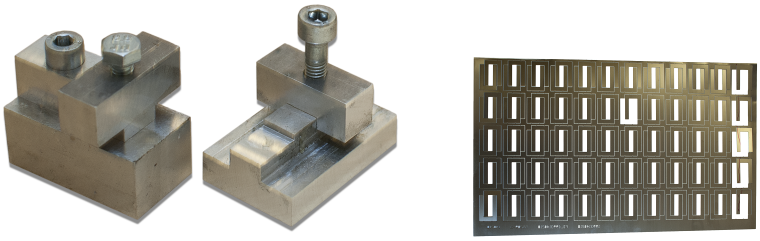

(a) Photo of stacking aids

(b) Photo of the core plates as delivered by supplier

Figure 3.9: Pictures of the mumetal sheets purchased and the aids used for stacking those on top of each other

Neodymium magnets with a magnetisation level of 900 kA/m [21] were purchased and later glued to the magnet holder using Loctite cylindrical glue. Another Loctite product with activator was used to attach the spring to the magnet holder. Overall, a column of about 0.1 mm was used to make room for the glue.

Since the bobbin had to be electrically insulating, plastics was the obvious choice of material. Using rapid prototyping or 3D printing as means of manufacturing was an advantage by many reasons. Most importantly, it provided a fast and cost-effective way of producing a small test series of complex geometries. By using a 3D-printing technology based on thermosetting plastics, fine tolerances were obtained. This means that during the design of the test object there was no need to consider the case of the machine not being able to produce the level of detail needed.

The assembled bobbins with metal cores were shipped to a manufacturer for rolling the coil onto the bobbin. Outsourcing this manufacturing event ensured high packing density and correct amount of wire to be rolled onto each bobbin. Using the right tooling for the job also ensured that no damage was made to the wire, which was essential with regard to the limited time. The assembled product is shown in Figure 3.10.

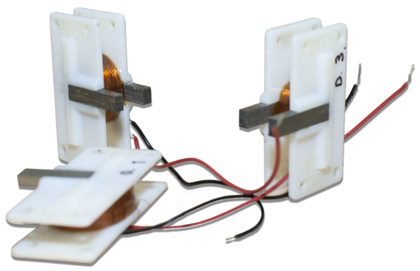

Figure 3.10: Photo of assembled bobbins

3.5 Execution of test

Mentioned earlier, the factors to be tested for their effect on the outputted power of the VEH were the magnet size, the wire diameter, and the lamination thickness. Testing these factors at two different levels through a full factorial design resulted in eight individual tests. These different set-ups were in turn tested at four different loads and consequently the total amount of measurement points ended at 32.

The tests were executed in the Vibration Lab in the M-building at Chalmers. The equipment used was not originally designed for the purpose but was considered the best option available at the time. An electric motor with a de-centred axle provided a minimum displacement A of 1.5 mm and the frequency could be varied by changing the speed of the motor. Figure 3.11 shows how the test rig was mounted onto this device.

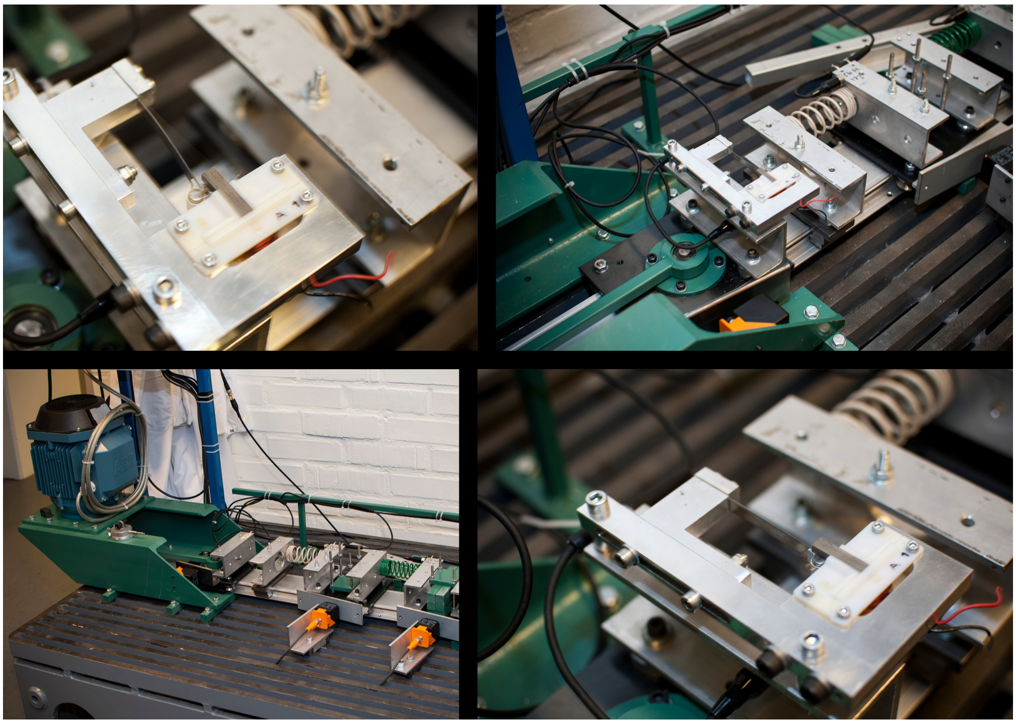

Figure 3.11: Photos from testing day showing how the test equipment was mounted onto the shaking device

Tuning the shaking device for 1.5 mm amplitude and vibration frequency f of 60Hz, Equation (2.3) gives the maximum acceleration $a_{\max}$ as

$$a_{\max} = |-(2\pi f)^2 A| = 213.18 \text{ m/s}^2 \tag{3.4}$$

and thus the RMS acceleration level during the test was

$$a_{\text{RMS}} = \frac{a_{\max}}{\sqrt{2}} = 150.74 \text{ m/s}^2 \tag{3.5}$$

The power of the VEH was estimated by adding a load to the circuit and measuring the voltage using an oscilloscope (see Appendix D). In this case, the RMS voltage represented the voltage given after rectification and thus the usable voltage. The power was calculated by using Ohm's law according to

$$P = \frac{U_{\text{RMS}}^2}{R} \tag{3.6}$$

3.6 Test results

The measurement data acquired during testing are presented in Table 3.5. In order to give an indication of how the VEH performed at different loads, the voltage was measured unloaded and at 10Ω, 100Ω, and 1000Ω.

Table 3.5: Collected measurement data from the eight test runs

		Voltage [U_{RMS}]			
Experiment nr.	Run nr.	∞ Ω	10 Ω	100 Ω	1000 Ω
1	5	5.78	0.872	3.76	5.59
2	2	7.21	0.78	4.03	6.74
3	7	1.37	0.66	0.87	0.87
4	6	1.69	1.17	1.63	1.67
5	1	8.26	0.35	5.06	7.95
6	3	9.63	0.96	5.33	9.29
7	8	1.91	1.47	1.92	1.9
8	4	2.31	1.59	2.24	2.32

For these different loads, the power was calculated using Equation 3.6. In Figure 3.12(a), the results are plotted over the different loads. In the diagram, it is clearly observed that four experiment set-ups, namely 3, 4, 7, and 8 were experiencing its maximum power at the low 10Ω load. The remaining configurations were achieving maximum performance at the 100Ω load.

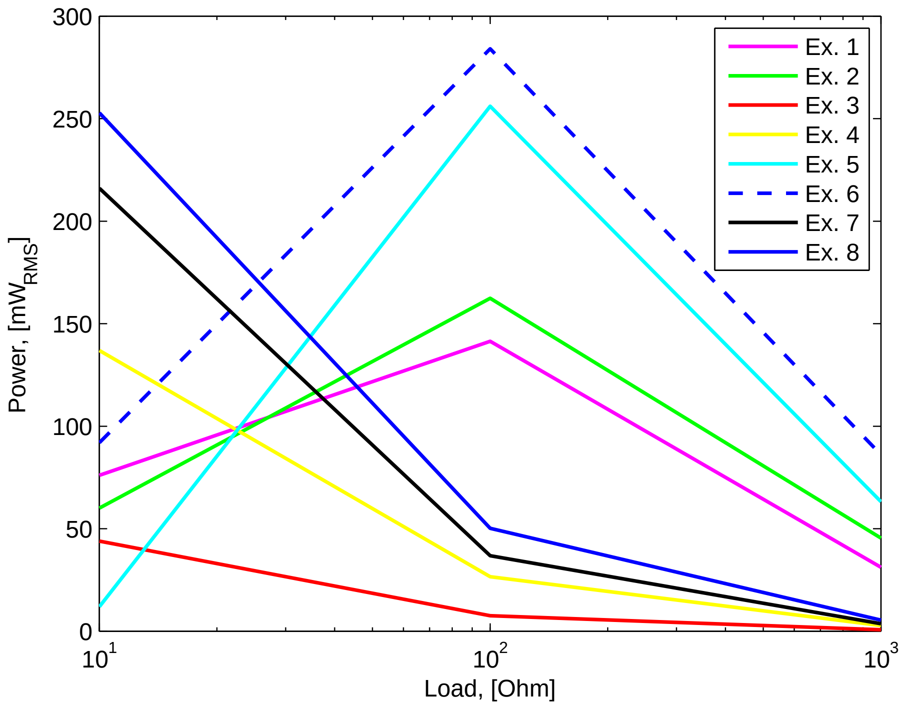

(a) Calculated power

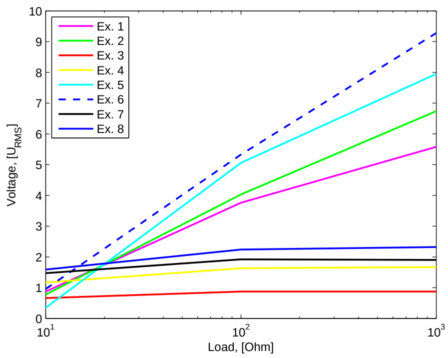

(b) Measured voltage

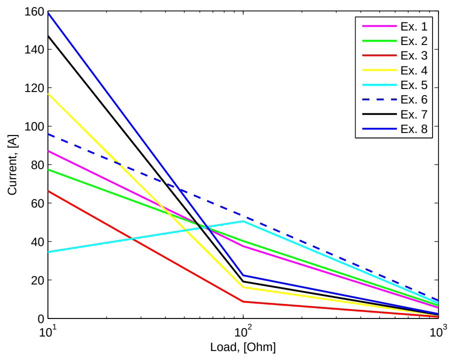

(c) Calculated current

Figure 3.12: Test results for each experiment configuration at 10, 100, and 1000 Ω load

The configuration generating the highest power according to Figure 3.12(a) was Ex.6, which according to Table 3.3 had the following properties:

- High level magnet length (10 mm)
- Low level wire diameter (0,2 mm)
- High level lamination thickness (0,4 mm)

The produced power at 100 Ω was around 280 mW, which was far above the expectations. Illustrated in Figure 3.12(b) experiment number 6 was the best performing in terms of output voltage but also the current passing through the coil (3.12(c)). Based on these results and the fact that 100 Ω seemed equivalent to the resistance of the RF-technology of Upwis, this was the response variable chosen to be subject for the DOE analysis. In other words, the updated design matrix formed as illustrated in Table 3.6 below.

Table 3.6: DOE Design Matrix with updated response variable

		Factors							Response
Experiment nr.	Run nr.	A	B	C	AB	AC	BC	ABC	$P_{100\Omega}$ [mW]
1	5	-1	-1	-1	1	1	1	-1	141.38
2	2	1	-1	-1	-1	-1	1	1	162.41
3	7	-1	1	-1	-1	1	-1	1	7.60
4	6	1	1	-1	1	-1	-1	-1	26.57
5	1	-1	-1	1	1	1	1	1	256.05
6	3	1	-1	1	-1	-1	1	-1	284.09
7	8	-1	1	1	-1	1	-1	-1	36.87
8	4	1	1	1	1	-1	-1	1	50.18

The estimated effect or Contrast of a factor is given by subtracting the average result when the factor's level is low from the average result when the level is high. The general formula for Contrast is given as

$$\text{Contrast} = \frac{\sum_{i=1}^{\frac{n}{2}} y_i^-}{\frac{n}{2}} - \frac{\sum_{i=1}^{\frac{n}{2}} y_i^+}{\frac{n}{2}} = \frac{\sum_{i=1}^{\frac{n}{2}} \pm y_i}{\frac{n}{2}} \tag{3.7}$$

The calculated Contrasts are given in Table 3.7 below.

Table 3.7: Calculated Contrasts

Factor	Contrast
Magnet length	10.17
Wire diameter	-90.34
Lamination thickness	36.15
Magnet length · Wire diameter	-2.10
Magnet length · Lamination thickness	0.17
Wire diameter · Lamination thickness	-22.93
Magnet length · Wire diameter · Lamination thickness	-1.58

The normal probability plot in Figure 3.13 illustrates the contrasts that will affect the generated power the most. These are the *Wire diameter*, the *Lamination thickness*, and the interaction between these two.

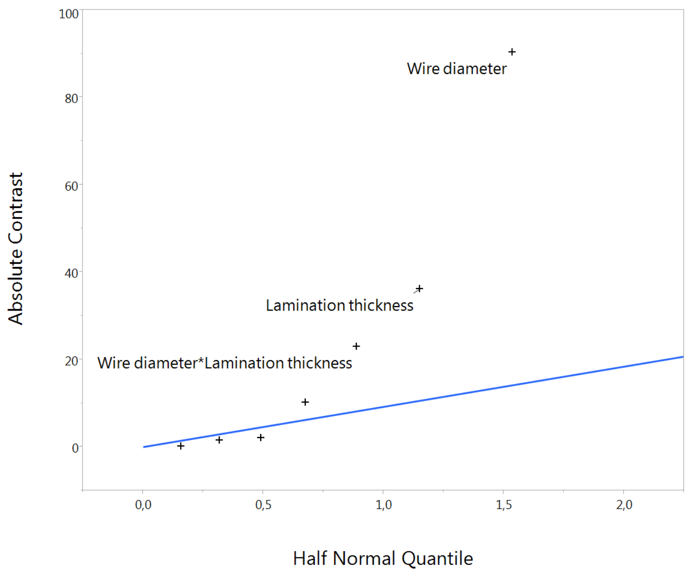

Figure 3.13: Normal probability plot indicating which are the active factors

The only existing active interaction identified was between lamination thickness and wire diameter. Figure 3.14 shows the behaviour of the interaction and thus pictures how combinations of high and low levels of the two factors affect the response. This states that maximum power is achieved when combining low level on wire diameter with high level on lamination.

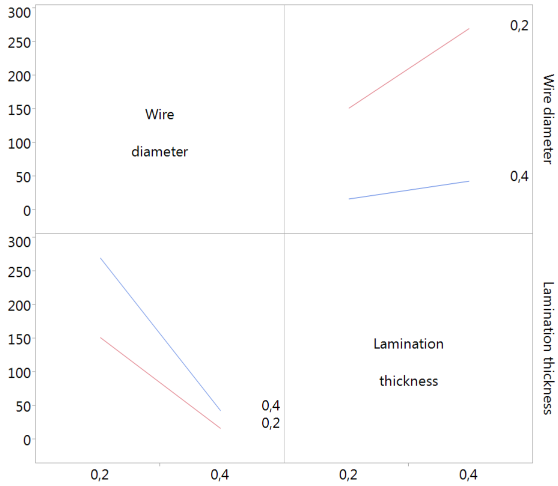

Figure 3.14: Interaction plot showing the dependency between the two active factors

3.6.1 Interpretation and discussion on results

The overall conclusion from the experiments was that the diameter of the coil wire and the lamination thickness were the two variables out of the three having significant effect on the performance. Furthermore, arranging and performing the test gave valuable knowledge about the technology in itself that helped in identifying the real weaknesses with the concept. Some other conclusions are:

- No estimation of the experimental error was made, which could be done by replicating the runs and calculating the sample mean value.
- The lack of third-order interactions speaks for changing the full factorial design for a fractional factorial design and thus enabling more factors to be tested given the same sample size.
- Testing each factor at more than two levels would allow for better interpolation of irregular behaviours of the VEH that could help in future optimisation work.
- The reason to why the magnet length did not show as an active factor may be related to the fact that this factor was not entirely decoupled the rest of the design. Fact is that the length of the magnet determines the width of the bobbin and thereby the number of wire turns that can be fitted onto the same.
- The excitation source used for the experiment provided a very high acceleration level that may not be representative for a real-life scenario.

3.7 Second generation prototype proposal

The prototype development process resulted in a design proposal for a second generation prototype. This was based on the best performing set-up from the testing since there was no time for another iteration. The properties of the proposal are listed in Table 3.8.

Table 3.8: Properties for prototype proposal

Item	Material	Dimensions	Mass	Young's modulus
Beam	SS1770-04	L=52.27 mm, w=7 mm t=0.7 mm	2 g	208.5 GPa
Magnet	NdFeB	L=10 mm, d=6 mm	2.1 g	-
Magnet holder	EN7075	h=14.5 mm, w=7 mm	0.97 g	-
Coil	copper	d=0.2 mm, N=1890	-	-
Core	mumetal	t=0.4 mm, h=6 mm w_{o}=18.6 mm, w_{i}=10.6 mm	-	-

In order to make the prototype sustaining the harsh environment of railways tracks and other, a plastic casing was designed to protect it. The casing was designed in a way that the harvester is fixed and cannot move when placed inside it. Figure 3.15 shows how the dimensions of the proposal falls into the range of the specification (see Appendix C) in all directions but one. However, according to the customer the width was the least critical measure and thus exceeding this dimension did not cause any inconvenience.

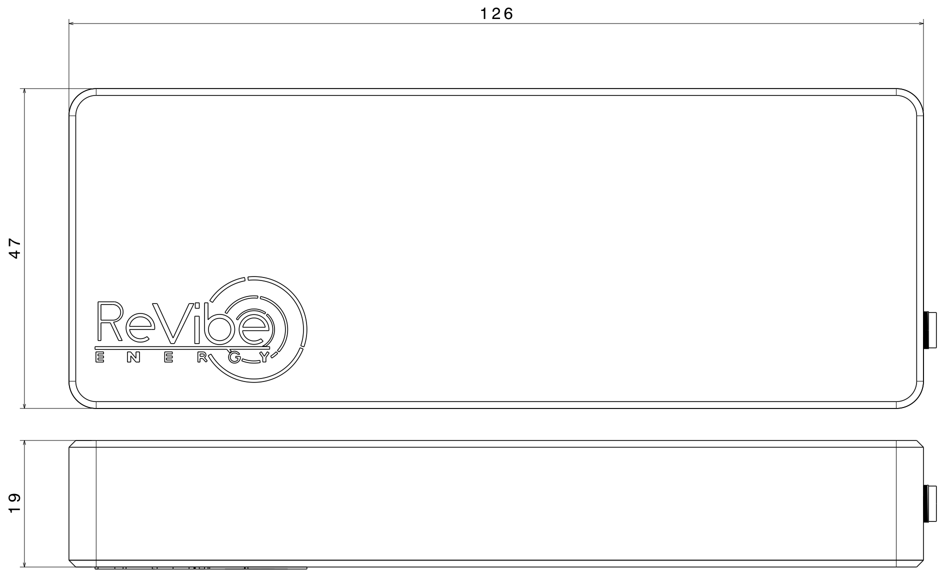

Figure 3.15: Illustration showing the overall dimensions in mm of the proposed design

The fixture constituting the foundation of the device was designed with a minimum number of parts to enable for easy manufacturing. It has pieces of hard rubber limiting the maximum deflection of the beam. This measure was adjusted according to what was observed as maximum deflection during testing. Based on the fact that this measure varied it was set to the mean value being 7.7 mm.

Figure 3.16 illustrates the design proposal.

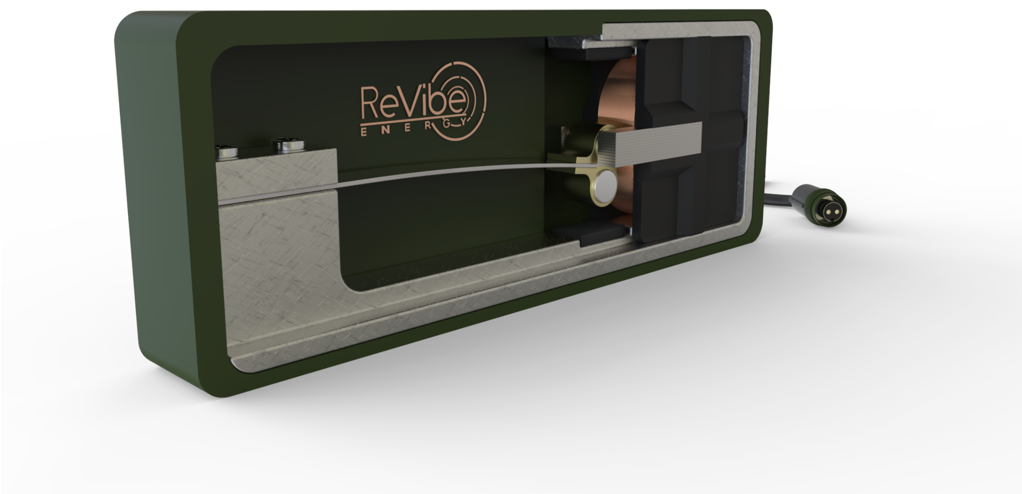

(a) The proposal holds a connector for attachment to sensor node

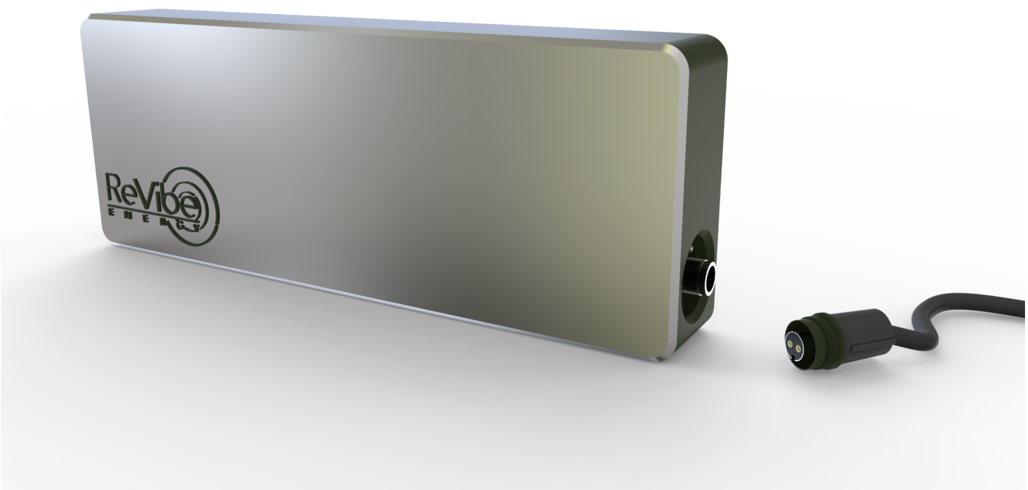

(b) The durability of the VEH is assured by protecting it from dirt and corrosion

Figure 3.16: Design proposal of 2nd generation prototype

4

Simulations and numerical modelling

This chapter concerns the identification of vibrational pattern and the creation of a numerical model to simulate the behaviour of the VEH. It starts with an analysis of accelerometer data obtained from the suspension of a cargo train wagon and is followed by some performance analyses of the device.

4.1 Analysis and interpretation of gathered vibration data

An outcome from the cooperation with Upwis was that accelerometer data was obtained from a real freight train. This accelerometer data was analysed in order to determine the frequency distribution and the acceleration level of the vibrations present in this environment.

4.1.1 Frequency intensity

To determine the driving frequency of the vibrations a spectral analysis was performed in Matlab using the tool *spectrogram*. This returns the short-time Fourier transform of the input signal. In Figure 4.1, the intensity of different frequencies of the acceleration data are plotted as a function of time.

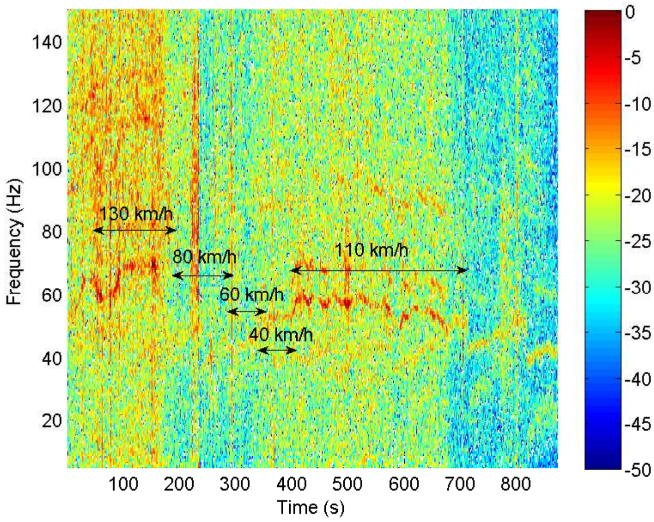

Figure 4.1: Spectral analysis illustrating where the power spectral density dominates at the different vibration frequencies

From Figure 4.1 it is clear that the driving frequency is close to 60Hz when the train has a velocity of somewhere between 110 and 130 km/h. In order to estimate the vibration level at these occasions, the time sequence (Time=52 - 62 s) was selected for analysis (see Figure 4.2).

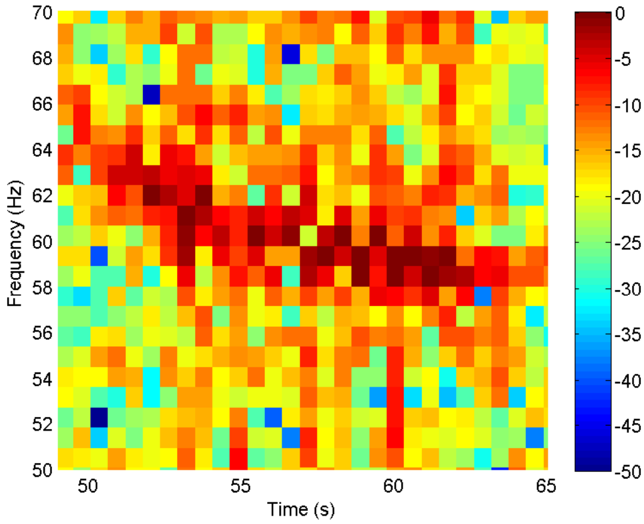

Figure 4.2: Enlargement of frequency spectrum for the chosen interval

4.1.2 Vibration level in frequency region

According to theory the productive frequency range of the VEH is a few Hz and in line with this the bandwidth was assumed to be 5 Hz. With this assumption the vibration level present in this frequency region could be quantified. The RMS acceleration in frequency regions with a length of 5 Hz was calculated with a MATLAB-script, see Appendix A, and is illustrated in Figure 4.2. This clearly shows that the RMS acceleration is peaking in the frequency region 57.5 - 62.5 Hz, where $a_{\mathrm{RMS}} = 0.59$ m/s^2.

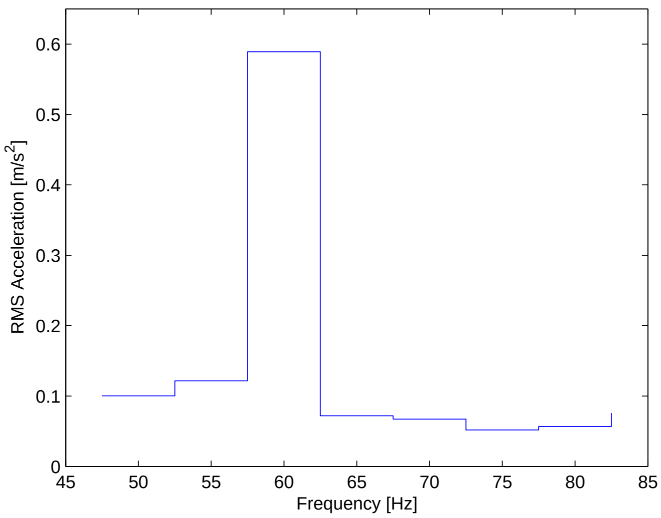

Figure 4.3: Freight train acceleration level in different frequency regions, assumed bandwidth = 5Hz

4.2 FE-Model of the electromagnetic subsystem

When the magnets oscillate relative to the mumetal core they will experience magnetic forces which in turn will counteract the movement of the magnets and hence the deflection of the spring. To fully quantify the magnitude of these forces in a time dependent system is, however, cumbersome and hard. In order to succeed with this task some assumptions and simplifications had to be made. The electromagnetic subsystem was modelled and analysed using Comsol Multiphysics®.

4.2.1 Assumptions

In the created model the core was given the properties of Comsol's built in material *soft iron, no losses* which is a linear material without hysteresis and eddy current loss. In reality this would never be the case, but when using thin laminations of mumetal the internal losses in the core are drastically reduced and the approximation therefore seemed legitimate. Further, using a material with no internal losses allowed for the more simple *steady-state* analysis to be used instead of a *time-dependent* analysis, which also consider the dynamic behaviour of the system. The material of the core was assigned the same relative permeability μ_{R} as that of ordinary mumetal, 20000 [16]. The magnets were given a the same magnetisation level as those used in the experiment, namely 900 kA/m [21]. In this model the dimensions of the core and magnets were the same as those of the prototype proposal described in *Section 3.7*.

4.2.2 Parametric sweep and evaluation of magnetic forces

With the assumptions stated above, the analysis could be performed in the *Magnetic Fields, No Currents* interface and a parametric sweep was used to evaluate the force acting on the magnets at different positions. A fine mesh was used for the core and magnets and an additional mesh refinement was performed on the boundaries between the magnets and the core. For the surrounding air a normal sized mesh was used. Some of the positions analysed are illustrated in Figure 4.4.

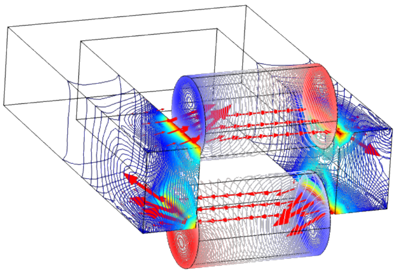

(a) At its equilibrium position, the opposite polarity of the magnets will prevent any magnetic field to pass through the core

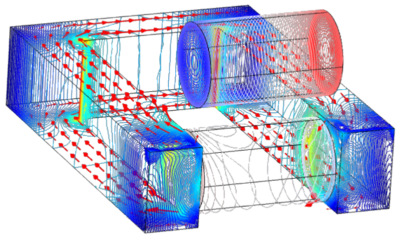

(b) The magnetic field in the core is the strongest when affected by one magnet at the time

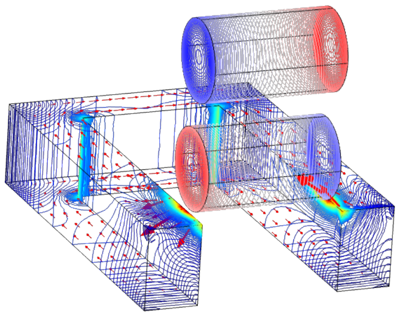

(c) As the magnets move away from the core the magnetic field between magnet and core will counteract the movement

Figure 4.4: Illustration of some positions of the parametric sweep made in Comsol Multiphysics, where the magnetic flux through the core is calculated and the resulting magnetic force is evaluated.

In the parametric sweep the forces between the magnets and the core were calculated by Comsol Multiphysics. These forces were calculated at positions of 20 mm in each direction from the core with a step size of 0.05 mm. This resulted in 800 collected data points according to the graph illustrated in Figure 4.5.

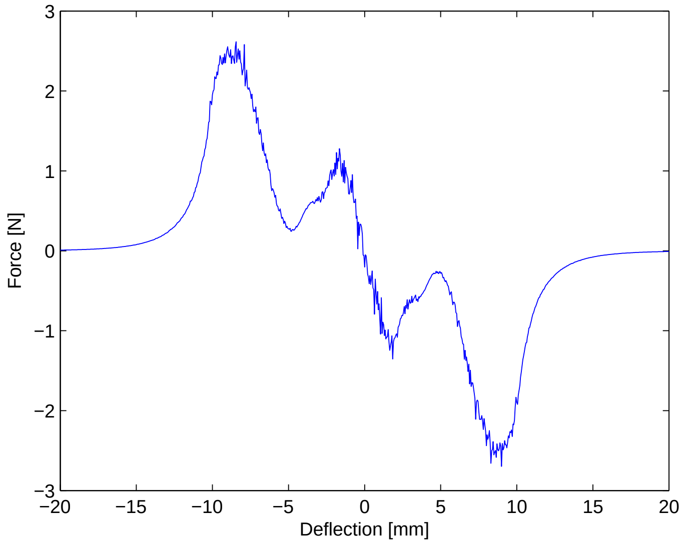

Figure 4.5: The electromagnetic force acting on the magnets as a function of the tip mass deflection

4.3 FE-model of the mechanical subsystem

From the physical tests it was concluded that the limitations of the VEH mainly were related to the beam's ability to oscillate. As the VEH was tested in rather optimal conditions the question remained how it would behave in real life conditions. The most important question to answer was; In what frequency range could the VEH generate power and at what acceleration level? In order to answer these questions it was essential to model the behaviour of the oscillating beam as accurate as possible. This was done using the *harmonic oscillation* and *transient structural mechanics* modules in Ansys.

4.3.1 Translation of electromagnetic forces

Including the electromagnetic forces in the FE model required those to be translated from position-dependency into a function of time. This was done by assuming and amplitude and frequency of the tip mass and matching position with time. For the analysis of the damping ratio (which will be discussed in *Section 4.3.3.1* it was beneficial to represent the forces as a periodic function rather than as discrete data points. Matlab's function *cftool* made it possible to construct a function consisting of sine terms that was close to identical to the force data. The sum of sines model used gave

$$y = \sum_{i=1}^{n} a_i \sin(b_i x + c_i) \tag{4.1}$$

where a is the amplitude, b the angular frequency, and c is the phase constant for each wave term [22]. As the number of terms is increased the accuracy of the periodic model increases. In Figure 4.6 one period of the magnetic force together with the fitted periodic function are illustrated. The tip mass amplitude was given the value that was observed during the test at its resonance frequency, namely 5 mm at a frequency of 60Hz.

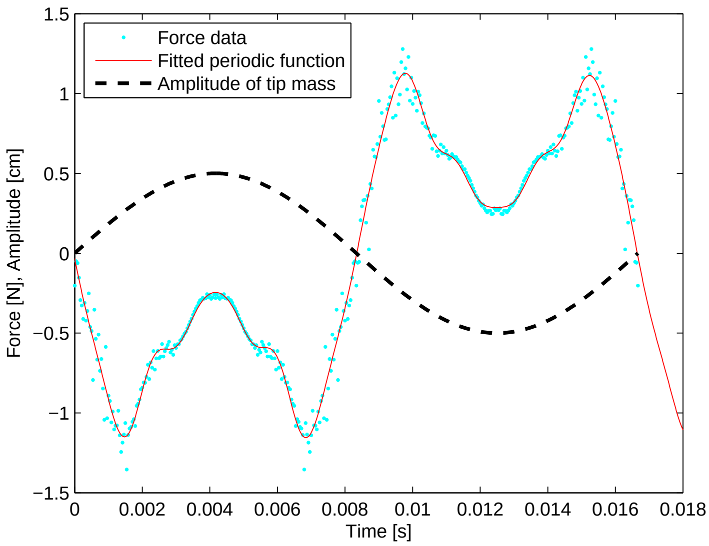

Figure 4.6: Periodic function used to model the magnetic forces

The sum of sine model used gave

$$\begin{aligned} f(x) = {} & a_1 \sin(b_1 x + c_1) + a_2 \sin(b_2 x + c_2) + a_3 \sin(b_3 x + c_3) + \\ & a_4 \sin(b_4 x + c_4) + a_5 \sin(b_5 x + c_5) + a_6 \sin(b_6 x + c_6) + \end{aligned} \tag{4.2}$$

with coefficients presented in Table 4.1.

Table 4.1: Coefficients of fitted curve function.

N	1/s	
$a_1 = 0.7825$	$b_1 = 376.5$	$c_1 = -3.144$
$a_2 = 0.5867$	$b_2 = 1130$	$c_2 = -3.132$
$a_3 = 0.1172$	$b_3 = 1877$	$c_3 = -3.064$
$a_4 = 0.07749$	$b_4 = 3375$	$c_4 = 0.1094$
$a_5 = 0.03069$	$b_5 = 4889$	$c_5 = -3.043$
$a_6 = 0.02074$	$b_6 = 3731$	$c_6 = -1.371$

4.3.2 Assumptions and input to Ansys

With the aim of simulating the relative amplitude $z(t)$ of the spring tip mass when the device is subjected to the displacement $y(t)$, some assumptions and simplifications were made. Firstly, the fixture was assumed to be rigid and with negligible weight compared to the surrounding vibration source. Secondly, any mechanical damping within the spring was neglected. Lastly, the excitation source was given the shape of a sinusoidal curve with amplitude A and angular frequency Ω, see Figure 4.7.

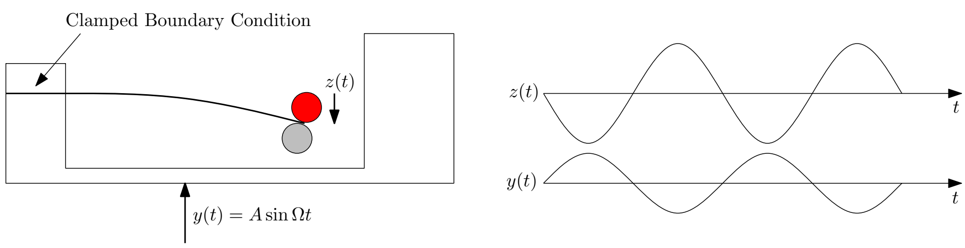

Figure 4.7: Illustration of the relationship between excitation amplitude and tip mass amplitude

With these assumptions the entire VEH was not needed to be modelled. Instead, a displacement was applied directly on the end of the clamped beam, see Figure 4.8.

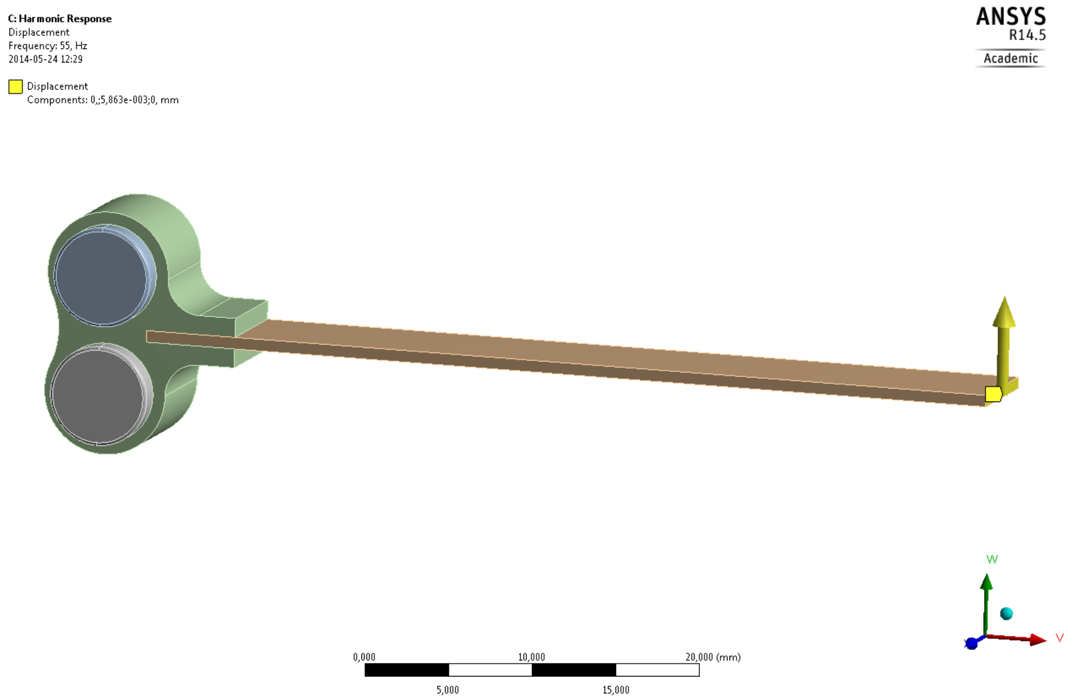

Figure 4.8: A time harmonic displacement is applied at the end of the beam to simulate the excitation

4.3.3 Harmonic Response

In order to analyse the stationary behaviour of the VEH, which occur when the tip mass amplitude have reached a constant level, the *Harmonic Response* module in Ansys was used. The input to the harmonic response was the amplitude and frequency of the excitation source and the magnetic forces acting on the tip mass. To analyse the amplitude of the tip mass in different frequencies a parameter sweep between 55 and 65 Hz was used. As the analysis was made in stationary conditions, the magnetic forces represented by Equation 4.2 was simplified to only include its first term as it will dominate at frequencies around 60Hz. Hence, the force equation used in the harmonic response was

$$f(t) = a_1 \sin(b_1 t + c_1) = 0.7825 \sin(376.5t - 3.136) \text{ N} \tag{4.3}$$

4.3.3.1 Estimation of damping ratio

As discussed in *Section 2.4.1*, it is beneficial to express the magnetic forces as damping in the system for making the model less complex. In this case the electromagnetic force acting on the magnets was translated into a damping coefficient that would predict the response of the system more accurate compared to the undamped case. The VEH was modelled as a SDOF-system with a stationary harmonic excitation source with a fixed frequency. With this estimation it was possible to express the damping coefficient as

$$F(t) = cv(t) \tag{4.4}$$

for a fixed frequency ω, where

$$F(t) = \hat{F}\mathrm{e}^{\mathrm{i}\omega t},\ v(t) = \frac{\mathrm{d}y}{\mathrm{d}t} = \mathrm{i}\omega A\mathrm{e}^{\mathrm{i}\omega t} \tag{4.5}$$

Here $\hat{F}$ is the amplitude of the force and is assumed to be equal to a_1 from Equation 4.3 and A is the tip mass amplitude. Equation 4.4 and 4.5 give

$$c = \frac{F(t)}{v(t)} = \frac{\hat{F}\mathrm{e}^{\mathrm{i}\omega t}}{\mathrm{i}\omega A\mathrm{e}^{\mathrm{i}\omega t}} \tag{4.6}$$

Given the damping coefficient c the damping ratio ξ is given as

$$\xi = \frac{c}{2m\omega} \tag{4.7}$$

With $A = 0.005$ m, $\hat{F} = 0.7825$ N, $f = 60$ Hz and $m = 0.0075$ kg the damping ratio was given as

$$\xi = \frac{0.7825}{2 \cdot 0.0075 \cdot 0.005(2\pi \cdot 60)^2} = 0.0734 \tag{4.8}$$

Hence the corresponding damping ratio is 7.34%.

4.3.3.2 Excitation amplitude from test

To verify the model the same excitation amplitude used during testing (1.5 mm) was applied. With damping ratio according to Equation 4.8, the frequency response of the tip mass amplitude in the interval of 55 to 65Hz was analysed. The resulting response is presented in Figure 4.9.

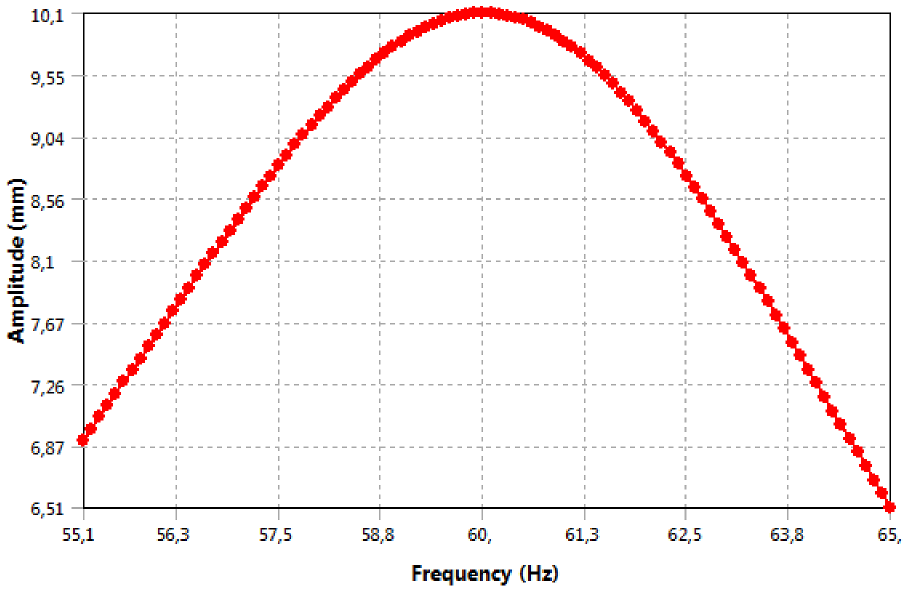

Figure 4.9: Frequency response from 55 to 65Hz with 1.5 mm excitation amplitude and damping ratio of 7.34 %

According to Figure 4.9, the tip mass of the beam will have high enough amplitude to generate power in the range of 55 to 65Hz. This conclusion matched the observations made during the tests and thus gave an indication of the validity of the FE-model.

4.3.3.3 Excitation amplitude from freight train data

To determine whether the current design of the VEH would generate any power in the conditions present in the freight train environment the measured acceleration level was translated into a displacement according to

$$a_{\mathrm{RMS}} = \frac{(2\pi f)^2 A}{\sqrt{2}} \Rightarrow A = \frac{a_{\mathrm{RMS}}\sqrt{2}}{(2\pi f)^2} = \frac{0.5892\sqrt{2}}{(2\pi 60)^2} = 0.0059 \text{ mm} \tag{4.9}$$

This was done for a fixed frequency of 60Hz and the amplitude gave a frequency response of the tip mass illustrated in Figure 4.10.

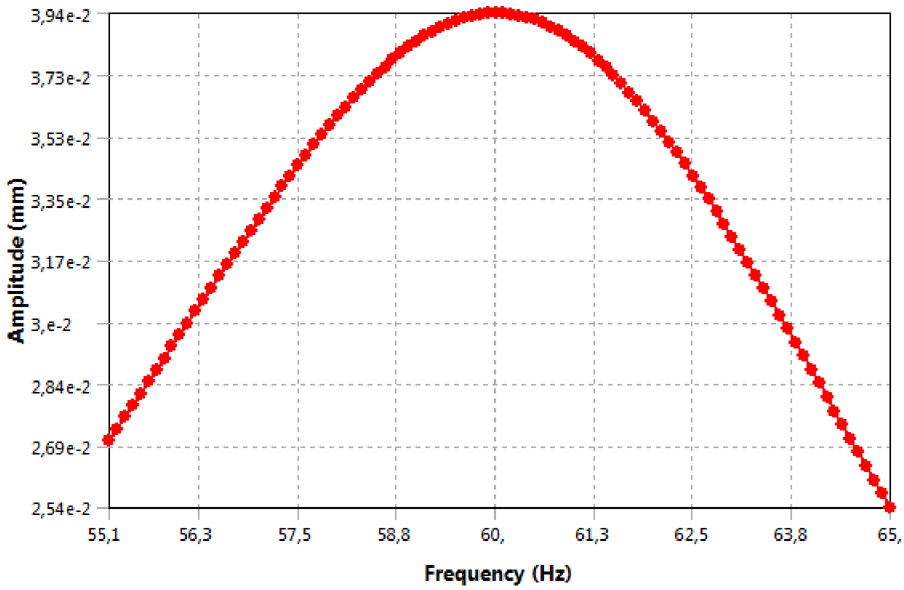

Figure 4.10: Frequency response from 55 to 65Hz with 0.0059 mm excitation amplitude and damping ratio of 7.34%

As illustrated in the graph, the tip mass amplitude is extremely low at all frequencies within the range, even at its natural frequency. Hence, the analysis indicated that the VEH's current design would not generate any power in the freight train environment.

4.3.4 Transient analysis

If the VEH is to generate any power at all it is crucial for the beam to start oscillating. But, if the magnetic force is too strong it will lock out every small oscillation and the beam will stay at rest. For analysing these initial conditions of the beam, Ansys module *Transient Structural* was used. Figure 4.11 illustrates the tip mass displacement given when applying freight train conditions, starting at time $t = 0$.

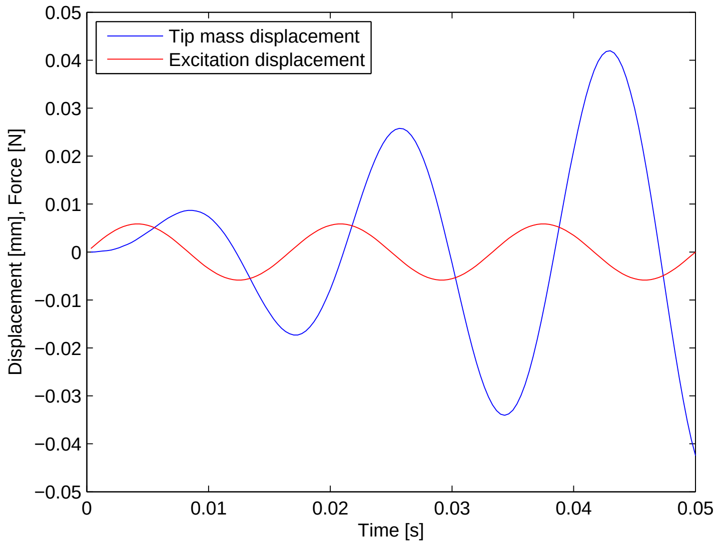

Figure 4.11: Initial behavior of beam when affected by a sinusoidal vibration with amplitude and frequency according to freight train data

For applying the correct magnetic force at every discrete displacement of the tip mass a Matlab-script was created to match the displacement data from Ansys to the magnetic force data from Comsol Multiphysics. As illustrated in Figure 4.12,when the tip mass amplitude is low the magnetic force follows a linear behaviour.

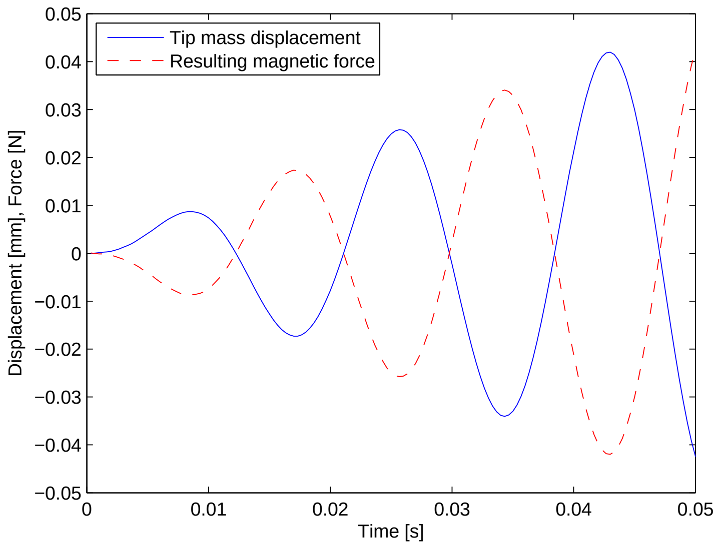

Figure 4.12: Graph showing the corresponding magnetic force acting on the tip mass as a function of displacement

The resulting magnetic force was used in Ansys together with the previous input to predict the initial behaviour of the beam. Figure 4.13 illustrates the first period of this run and it shows that the oscillation of the beam is damped but nevertheless starts.

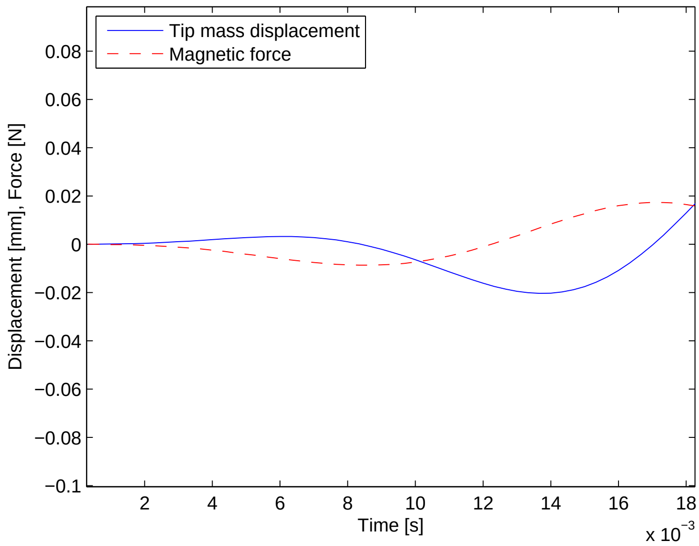

Figure 4.13: The graph illustrates the first sequence of the beam deflection as it experience an ambient vibration and the tip mass is subjected to counteracting magnetic forces

4.4 Simplified model in Matlab

If the VEH could be expressed as the mass-spring-damper system explained in *Section 2.4* the simulations and analyses could be performed a lot quicker and would be easier to configure. Using Matlab, a mass-spring-damper system was modelled and the tip mass amplitude was given at different frequencies and excitation amplitudes. In Figure 4.14 the responses from the Matlab model and the Ansys model are compared, in this case with a damping ratio ξ of 7.34 % and excitation amplitude A of 1.5 mm.

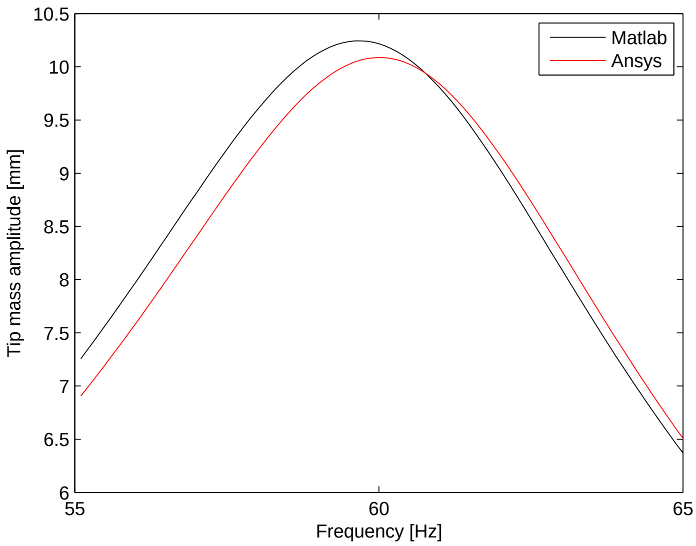

Figure 4.14: The tip mass amplitude in MATLAB vs ANSYS when an excitation amplitude of 1.5 mm and damping ratio of 7.34 % are used

As the graph indicates the simplified model used in Matlab corresponds well to the numerical FE-model used in Ansys. Several different configurations were compared and the conclusion was that the simplified model was sufficient for describing the mechanical behaviour of the VEH.

4.4.1 Responses at different vibration levels

As mentioned repeatedly throughout this report the amplitude of the tip mass on the beam has to be large enough if the VEH is to generate any power. It has also been stated that the excitation amplitude and frequency, who determine the vibration level, are strongly linked to the tip mass amplitude. The resulting tip mass amplitude at different excitation amplitudes is illustrated in Figure 4.15. The mass, damping ratio, and natural frequency of the VEH are given as input to the Matlab script, see Appendix A.

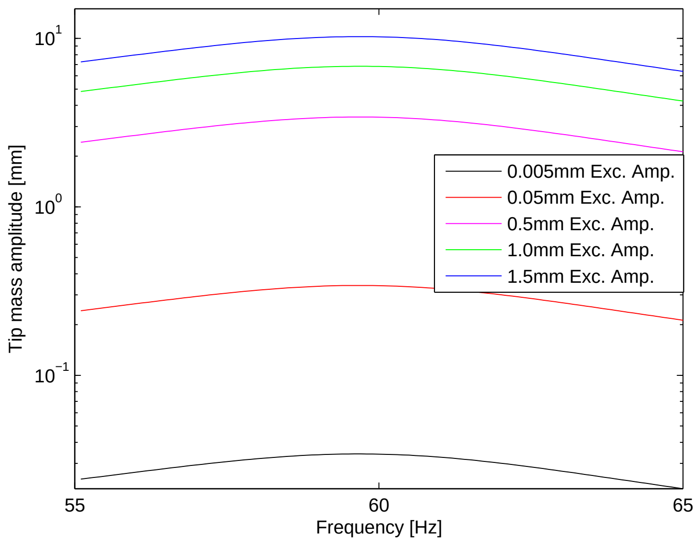

Figure 4.15: Mass-spring-damper model illustrating the tip mass amplitude given different excitation amplitudes

Figure 4.15 indicates that the tip mass amplitude would be high enough in order for the VEH to generate power at excitation amplitudes of 0.5 mm and higher.

4.4.2 Theoretical maximum power at different vibration levels

In *Section 2.4.1* Equation 2.24 gives an expression for the theoretical maximum power that the VEH could deliver at different excitation amplitudes, frequencies and damping ratios of the system. This expression was included in the Matlab-script and the theoretical maximum power output at each of the different excitation amplitudes shown above are illustrated in Figure 4.16.

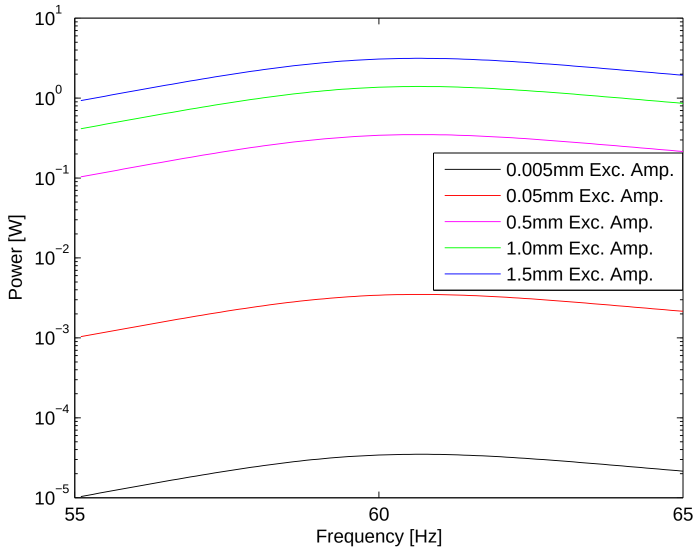

Figure 4.16: Theoretical maximum power available for extraction at different vibration levels

Figure 4.16 illustrates that the power available for extraction is around 3W for the excitation amplitude used during the tests (1.5 mm) and is around 30μW at the excitation amplitude in the freight train environment (0.0059 mm).

4.5 Fatigue and lifetime analysis

The principal idea behind changing batteries for energy harvesting technology is to minimise or eliminate the need for maintenance of the sensor node. Thus, a common selling argument for energy harvesting is extended lifetime compared to batteries that in turn can enable otherwise unsustainable network solutions.

In order to ascertain the expected lifetime of the VEH it is vital to analyse the stresses in the oscillating beam. Any structure being exposed to cyclic loads will face the risk of failure due to fatigue and this has to be taken into consideration in design. For the proposed design, the worst case scenario in terms of fatigue will occur when the beam is deflecting the most and hence experiences maximum stress. This will occur on the upper side of the fixed end of the beam. According to classic beam theory [23], the steady-state maximum stress is given as (fully reversed conditions)

$$\sigma_{\max} = \frac{F L}{I} \frac{h}{2} \tag{4.10}$$

where FL is the bending moment, h the thickness of the beam, and I is the moment of inertia. According to tabulated beam data, F and I are given as

$$F = \frac{p_{\max} 3EI}{L^3}, \; I = \frac{wh^3}{12} \tag{4.11}$$

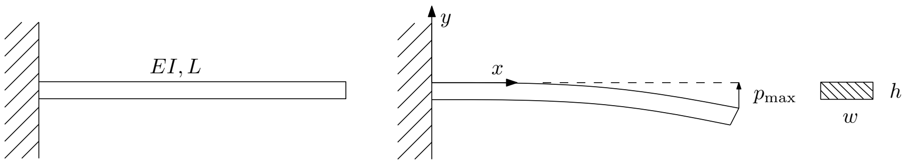

Figure 4.17: The maximum bending amplitude $\sigma_{\max}$ will occur at the fixed end of the beam during maximum deflection $p_{\max}$

The proposed design presented in *Section 3.7* had the following settings

- Beam length $L = 52.27$ mm
- Beam width $w = 7$ mm
- Beam thickness $h = 0.7$ mm
- Maximum deflection $p_{\max} = 7.7$ mm (restricted by the design)
- Young's modulus $E = 208.5$ GPa

these values provide a maximum bending stress amplitude of

$$\sigma_{\max} = \frac{3Ep_{\max}h}{2L^2} = 617 \text{ MPa} \tag{4.12}$$

where the deflection $p_{\max}$ is considered fully reversed. The beam material used for the developed prototype was the standard spring steel SS1770-04. This is not much unlike the Sandvik 15LM in composition and characteristics and thus using the $S - N$ curve for this material instead of the former was considered representative for determining the theoretical lifetime.

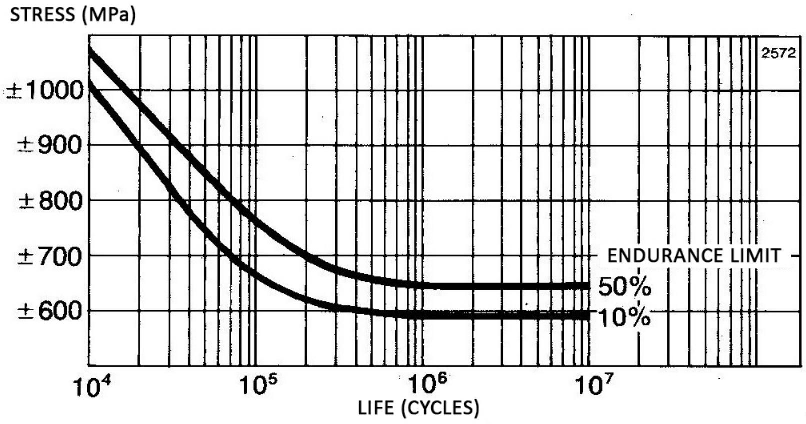

Figure 4.18: $S - N$ curve for a beam of the similar spring steel 15LM [24]

The $S - N$ curve in Figure 4.18 indicates that a stress level of 617 MPa will come with a probability of failure being higher than 10%. Since the lifetime is such an important design parameter for this kind of application, such a probability of failure is unacceptable. For secured functionality it is proposed to design for never going above 600 MPa in stress level. This would, at least in theory give an infinite lifetime of the beam. In this case, the beam is not carrying any load and therefore fatigue safety factor of 1.5 should be considered sufficient. This means that the maximum stress level would lie around 400 MPa. Also, there is no need for further reducing the fatigue due to surface conditions or material volume as perfectly polished conditions can be assumed and the beam height is very small.

It is important to note that the relationship presented in Figure 4.18 only is valid if the surface of the beam is polished and there is no defects such as scratches where a crack could propagate [23]. Also, the $S - N$ curve is only valid for perfectly clean environments. Exposing the device for any environment that somehow would affect its properties could drastically reduce the predicted lifetime.

4.5.1 Fatigue optimisation of mechanical subsystem

The identified fatigue issue combined with already existing requirements resulted in a trade-off situation between different properties of the mechanical subsystem. On the one hand, width, length, thickness, and material of the beam would determine the maximum bending stress and had to be adjusted in order to meet the 400 MPa limit. On the other hand, changing these parameters would directly affect the modal behaviour of the device. Thus, an optimum between the following two criteria had to be found

$$\begin{cases} f = 2\pi\sqrt{\frac{3EI}{mL^3}} = 60 \text{ Hz} \\ \sigma_{\max} = \frac{3Ep_{\max}h}{2L^2} \leq 400 \text{ MPa} \end{cases} \tag{4.13}$$

The upper of these requirements was first presented in *Section 2.3.1* as Equation 2.8. This is a simplified way of calculating the natural frequency of the mechanical subsystem based on the assumption that the tip mass is much larger than the mass of the beam itself. In other words, m is here referring to the mass of the beam tip exclusively. Finding the best combination of design parameters and at the same time fulfilling both these criteria called for creating some kind of optimising algorithm. The overall structure of the Matlab algorithm created is illustrated in Figure 4.19.

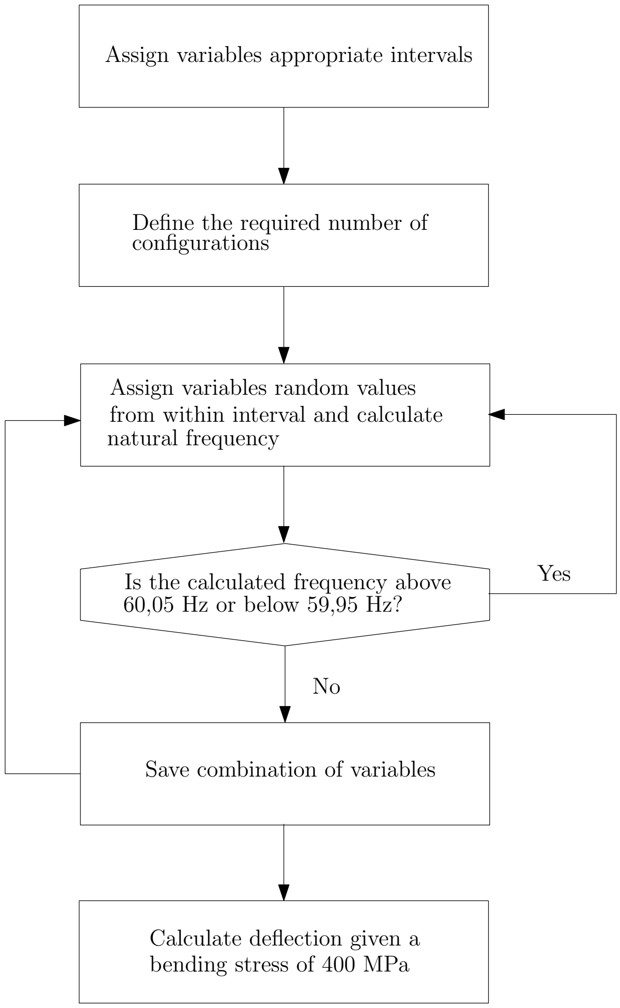

Figure 4.19: Basic structure of the algorithm used for identifying appropriate dimensions of mechanical subsystem

In brief, the algorithm picks random combinations of variables from within a given interval and checks whether the calculated natural frequency is close to 60 Hz. Those combinations who fulfil the criteria are registered and move on to the second stage where the maximum deflection is calculated based on the 400 MPa bending amplitude limit. The last part of the code presents the unique combination of beam length and thickness providing the largest deflection and thus also the highest theoretical power. It is to be noted that for this algorithm, the tip mass and spring material were set to be the same as used for the prototype. For the entire code, see Appendix A.

The generated combination giving maximum deflection and power while satisfying the conditions in Equation 4.13,was

- Beam length $L = 64.2$ mm
- Beam thickness $h = 0.88$ mm

These values provided a maximum allowable deflection of 5.97 mm, which is well within the range of what is needed. In conclusion, assigning these values to the design will assure a productive device with infinite life.

5

Discussion

In retrospect, the project has consisted in a great variety of activities spanning from heavy workshop manufacturing hours to pitching a business plan in an international competition. Throughout this journey, we have managed to meet all the dimensions of the purpose by completing the prototype delivery in time and creating a numerical model conforming to reality. Followed below are some discussions on the outcomes of the project.

5.1 Suitability in field

The analysis of the gathered accelerometer data combined with the numerical model resulted in the conclusion that the current configuration of the VEH is unsuitable for the intended purpose. It showed that the counteracting magnetic force was too high even for the highest acceleration level within the frequency spectra and thus the beam could not leave its equilibrium position. In conclusion, a redesign of the VEH is required for making it suitable for being put on train wagons.

The above statement was confirmed by executing a second round of tests using professional test equipment at Saab Training and Simulations in Huskvarna. This equipment provided the possibility to produce a vibration behaviour similar to the vibration data gathered. An interesting finding during this investigation was the fact that the first generation prototype actually performed better than the second at these vibrations. The main structural difference between these two set-ups is the stiffness of the beam and it seems like using a weaker beam allows for picking up irregular vibrations at low accelerations. Furthermore, the first generation prototype showed an ability to oscillate at frequencies further away from its resonance point than its successor.

It is clear that the limited bandwidth associated with most vibration energy harvesters is an issue. Numerical as well as empirical results have both confirmed that higher acceleration levels results in a larger bandwidth. In other words, facing low acceleration levels will require the ambient vibrations to have a constant frequency close to the natural frequency of the VEH. However, during the test mentioned above it was observed that when the beam first started to oscillate it could continue doing so at a wider frequency span than the analysis predicted. From this observation the conclusion was drawn that a major issue was to set the beam in motion.

Decreasing the magnetic force in terms of weaker magnets or enlarging the air gap may be solutions for enabling the beam to leave its equilibrium position. On the other hand, these measures will reduce the overall amount of energy that can be converted into electricity. Clearly, a trade-off between power generation and vibration sensitivity exists. How this relationship looks like is something that should be further investigated in order to estimate how much energy can be extracted from different levels of vibrations.

5.2 Validity of numerical models

For the FE as well as for the simplified model, the following assumptions where made in order to estimate the damping ratio determining the overall behaviour of the system

- Dynamic losses in the mumetal core were neglected
- The tip mass amplitude was assumed to be 5 mm in order to translate the position-dependent magnetic force into a time-dependent function
- Any existing mechanical damping in the system was neglected
- The first term of the curve fit was assumed dominant at stationary conditions
- The simplified VEH was modelled as a SDOF system with a stationary harmonic excitation source

With these assumptions combined with the physical properties of the prototype the numerical model gave results in accordance with the physical tests. However, during the tests mentioned above it was observed that very high acceleration levels were required in order for the tip mass to get an amplitude higher than 5 mm. This phenomenon is explained by the strong magnetic force restricting the tip mass at amplitudes above this level. In conclusion, the process of translating the magnetic forces into damping in the system will unavoidably lead to describing the system less detailed and losing some characteristics.

5.3 Sustainability aspects of monitoring train health

Only during the first four months of this year (2014), as many as 36 people have been killed or seriously injured on Swedish railways [25]. Monitoring the health of train wheels can reduce the damage made on the rails and thereby the number of accidents occurring in our society. Using energy harvesting as a power supply for these monitoring systems will add an ecological sustainability dimension; reducing the amount of batteries in the technosphere will reduce the ecological footprint.

In addition to the above, if the confidence in railway traffic could be increased by using this kind of systems the overall usage of the railways would also increase. So, if this could be achieved the environmental impact associated with the transportation of goods and people would be reduced.

5.4 Overall discussion

During this project it has shown very important to know the characteristics of the vibrations intended to be converted by the harvesting device. Knowing about the periodicity as well as the acceleration level of the vibrations is vital for successful tuning. It is therefore important to start investigating this before starting the detailed design of the harvester.

The proposed design has an estimated unlimited lifetime meaning it has a low probability of breaking due to fatigue. This estimation is based on a simplified model at stationary conditions as well as the assumption that the device is protected from harsh environments. This calls for encapsulating the device in a sealed casing fulfilling these requirements.

During this project, we have been exclusively responsible for developing the product of our employer Energy Harvesting Foundation. This means that we have not been able to seek technical expertise within the company but tried to solve the these challenges on our own. Thanks to the unique setting of the project we have learned how to ”bootstrap” i.e. get around problems on a small budget, and we have learned much about entrepreneurship as a whole.

6

Conclusion and Recommendations

The design of the VEH needs to be adjusted in order to be productive in the freight train environment. At its current design the counteracting magnetic force is too strong in order for the beam to leave its equilibrium position at these acceleration levels. Measures that could be taken for improving the responsiveness of the VEH are

- Reduce the damping ratio by changing the parameters affecting this
- Testing entirely different designs
- Use a less stiff beam
- Evaluate different ways of increasing the bandwidth

The numerical model predicts the behaviour of the VEH in a relatively accurate manner. However, the model is created on the basis of several assumptions and we can therefore not guarantee its accuracy in general settings. In order to assure the accuracy of the assumptions as well as the model, some of the following actions could be taken

- Include the dynamic core losses in the model
- Find a way of describing the magnetic force as discrete instead of a constant damping ratio
- Investigate the possibility of creating a fully coupled model describing the relationship between the electromagnetic and mechanical subsystem

Being a start-up company it is important to be both effective in efficient, that is to say doing the right things and doing them in the right way. From a product development perspective, we have identified some activities that could help getting in the right direction for the future

- Put resources on mapping and analysing vibration patterns in prospective environments
- Evaluate concepts virtually before physically
- Design a sealed casing in order to ensure durability
- Try to get hold of some hours in a good test facility and have a detailed plan for your tests
- Investigate how to match harvester with sensor node in order to optimise performance
- Quantify the importance of using a magnetic core

Bibliography

[1] *Wireless Sensor Network*. Wikipedia. 2014. URL: `http://en.wikipedia.org/wiki/Wireless_sensor_network`.

[2] S. Roundy, P.K. Wright, and J. Rabaey. "A study of low level vibrations as a power source for wireless sensor nodes". In: *Computer communications* 26.11 (2003), pp. 1131–1144.

[3] H. Okada and T. Itoh. "M-ary FSK Modulation Using Short Packet without a Preamble and Error Detection Codes for Low Power Wireless Communication". In: *Wireless Sensor Network* 6.3 (2014), pp. 35–42.

[4] D. Spreemann and Y. Manoli. *Electromagnetic vibration energy harvesting devices: Architectures, design, modeling and optimization.* Vol. 35. Springer, 2012, pp. 1–12.

[5] T. Galchev, H. Kim, and K. Najafi. "Micro power generator for harvesting low-frequency and nonperiodic vibrations". In: *Microelectromechanical Systems, Journal of* 20.4 (2011), pp. 852–866.

[6] R. Torah et al. "Self-powered autonomous wireless sensor node using vibration energy harvesting". In: *Measurement Science and Technology* 19.12 (2008), pp. 125–202.

[7] J. Twiefel and H. Westermann. "Survey on broadband techniques for vibration energy harvesting". In: *Journal of Intelligent Material Systems and Structures* 24.11 (2013), pp. 1291–1302.

[8] G. Takacs and B. Rohal. *Model Predictive Vibration Control.* Springer, 2012, pp. 25–64.

[9] T.L. Schmitz and K.S. Smith. *Mechanical vibrations: modeling and measurement.* Springer, 2011.

[10] R.K. Mobley. *Vibration fundamentals.* Butterworth-Heinemann, 1999.

[11] L. Tang, Y. Yang, and C. Kiong Soh. "Broadband Vibration Energy Harvesting Techniques". In: *Advances in Energy Harvesting Methods* (2013), pp. 17–61.

[12] C.B. Williams and R.B. Yates. "Analysis of a micro-electric generator for microsystems". In: *Sensors and Actuators A: Physical* 52.1–3 (1996). Proceedings of the 8th International Conference on Solid-State Sensors and Actuators Eurosensors {IX}, pp. 8 –11. ISSN: 0924-4247.

[13] S.P. Beeby, M.J. Tudor, and N.M. White. "Energy harvesting vibration sources for microsystems applications". In: *Measurement science and technology* 17.12 (2006), R175.

[14] A.R. Hambley. *Electrical Engineering: Principles and Applications*. Fifth Edition. Pearson Education, 2011. ISBN: 9780132130066.

[15] D.K. Cheng. *Field and wave electromagnetics*. Addison-Wesley series in electrical engineering. Addison-Wesley, 1989. ISBN: 9780201128192.

[16] X.C. Tong. *Advanced materials and design for electromagnetic interference shielding*. CRC Press, 2008.

[17] D. Jiles. *Introduction to magnetism and magnetic materials*. First Edition. Chapman and Hall, 1991. ISBN: 9780412386404.

[18] S.O. Kasap. *Principles of Electronic Materials and Devices*. McGraw-Hill, 2006. ISBN: 9780073104645.

[19] D.C. Montgomery. *Design and analysis of experiments*. John Wiley & Sons, 2008.

[20] Lesjöfors Fjädrar AB (In Swedish). *Teknisk Information*. 2014. URL: `http://www.lesjoforsab.com/teknisk-information/standard_stock_springs_catalogue_13_-_swedish_id1103.pdf`.

[21] *Magnetisation*. May 2014. URL: `http://www.supermagnete.de/eng/data_sheet_S-06-10-N.pdf`.

[22] MathWorks Inc. *Sum of Sines Models*. 2014. URL: `http://www.mathworks.se/help/curvefit/sum-of-sine.html` (visited on 04/14/2014).

[23] B. Sundström (In Swedish). *Handbok och formelsamling i hållfasthetslära*. Institutionen för hållfasthetslära, Kungliga Tekniska Högskolan, 1998.

[24] Lesjöfors Fjädrar AB (In Swedish). "S-N curve for 15LM steel". Provided by sales department via e-mail. May 2014.

[25] *Olycksstatistik (In Swedish)*. Trafikverket. 2014. URL: `http://www.trafikverket.se/Privat/Trafiksakerhet/Olycksstatistik/`.

A

Matlab code

```
%%%%%%%%%%%%%%%%%%%%%%%%%%%%%%%%
%Analysis of freight train data
%%%%%%%%%%%%%%%%%%%%%%%%%%%%%%%%

clear all
close all

load('matlab.mat')

%% Picking out acceleration matlab.mat
accX1146=(200/4096).*data_perpetuum_11_46_acc(:,1)';
accX1159=(200/4096).*data_perpetuum_11_59_acc(:,1)';
accX1221=(200/4096).*data_perpetuum_12_21_acc(:,1)';
accX1317=(200/4096).*data_perpetuum_13_17_acc800_pw2_100_goodtrack_acc(:,1)';
accX1406=(200/4096).*data_perpetuum_14_06_acc(:,1)';
%%
nfft=256*4;          %FFT length
win=hanning(nfft);   %Using Hanning Window
noverlap=nfft/2;     %The number of samples that each segment overlaps
fs=900;              %Sampling rate
%% Making Spectograms

[S,F,T,P] = spectrogram(accX1146,win,noverlap,nfft,fs);
[S1,F1,T1,P1] = spectrogram(accX1159,win,noverlap,nfft,fs);
[S2,F2,T2,P2] = spectrogram(accX1221,win,noverlap,nfft,fs);
[S3,F3,T3,P3] = spectrogram(accX1317,win,noverlap,nfft,800);
[S4,F4,T4,P4] = spectrogram(accX1406,win,noverlap,nfft,500);

%% Plotting frequency spectra

figure
subplot(5,1,1)
```

```
surf(T,F,10*log10(P),'edgecolor','none')
axis tight, view(0,90)
colorbar
caxis([-50 0])
ylim([5  150.0000])
xlabel 'Time (s)', title '10:56-11:56'

subplot(5,1,2)
surf(T1,F1,10*log10(P1),'edgecolor','none')
axis tight, view(0,90)
colorbar
caxis([-50 0])
ylim([5  150.0000])
xlabel 'Time (s)', title '11:54-11:59'

subplot(5,1,3)
surf(T2,F2,10*log10(P2),'edgecolor','none')
axis tight, view(0,90)
colorbar
caxis([-50 0])
ylim([5  150.0000])
xlabel 'Time (s)', ylabel 'Frequency (Hz)', title '12:05-12:21'

subplot(5,1,4)
surf(T3,F3,10*log10(P3),'edgecolor','none')
axis tight, view(0,90)
colorbar
caxis([-50 0])
ylim([5  150.0000])
xlabel 'Time (s)', title '12:49-13:17'

subplot(5,1,5)
surf(T4,F4,10*log10(P4),'edgecolor','none')
axis tight, view(0,90)
colorbar
caxis([-50 0])
ylim([5  150.0000])
xlabel 'Time (s)', title '13:35-14:06'
```

```
%%%%%%%%%%%%%%%%%%%%%%%%%%%%%%%%%%%%%%%%%%%%%%%%%%%%
%Calculation of RMS acceleration in frequency region
%%%%%%%%%%%%%%%%%%%%%%%%%%%%%%%%%%%%%%%%%%%%%%%%%%%%

clear all
close all

fs=900;         %Sampling rate
dflag='mean';

%% Fake signal to assure validity of program
f_energy=[47.5 52.5 57.5 62.5 67.5 72.5 77.5 82.5 87.5];
ters_lowf=1;
ters_highf=8;

t_fake=linspace(0,2,1800);

nfft=length(t_fake);
win=hanning(nfft);
noverlap=nfft/2;

f_fake=60;      %[Hz]
A_fake=sqrt(2)/(2*pi*f_fake)^2; % amplitude corresponding to 1gRMS@f_fake
acc_fake=(-(2*pi*f_fake)^2)*A_fake*sin(2*pi*f_fake*t_fake);

a_rms=max(abs(acc_fake))/sqrt(2);

[P_fake,Freq_fake]=psd(acc_fake,nfft,fs, win, noverlap, dflag);


%% Real signal data
load('matlab.mat')

accX1221=(200/4096).*data_perpetuum_12_21_acc(:,1)';

% Taking out dataintervall of interest
time=length(accX1221)/fs;
timestep=time/length(accX1221);
timevector=[0:timestep:time];

time_low=52;
tmp_low=abs(timevector-time_low);
[value_low idx_low]=min(tmp_low);
```

```
time_high=62;
tmp=abs(timevector-time_high);
[value_high idx_high]=min(tmp);

%Acceleration data from intervall of interest
accX1221_int=accX1221(idx_low:idx_high)

nfft=256*5;
win=hanning(nfft);
noverlap=nfft/2;

[P_real,Freq_real]=psd(accX1221_int,nfft,fs, win, noverlap, dflag);

%% Calculation of RMS Acceleration in frequency region
delta=1/fs;
P_fake=P_fake*delta;
P_real=P_real*delta;

%Pspecs_fake=P_fake(:,1);
Pspecs_real=P_real(:,1);

%Uses the function file traped.m to integrate and get E[a_RMS]
%rms_tot_fake=sqrt(2*traped(Pspecs_fake,Freq_fake));
rms_tot_real=sqrt(2*traped(Pspecs_real,Freq_real));

%f1_values_fake=(interp1(Freq_fake,rms_tot_fake,f_energy));
f1_values_real=(interp1(Freq_real,rms_tot_real,f_energy));

%ters_values_fake=diff(f1_values_fake(ters_lowf:ters_highf+1));
ters_values_real=diff(f1_values_real(ters_lowf:ters_highf+1));

%f0_ters_fake=f_energy(ters_lowf:ters_highf);
f0_ters_real=f_energy(ters_lowf:ters_highf);

x=[f0_ters_real(1)
   f0_ters_real(2)
   f0_ters_real(2)
   f0_ters_real(3)
   f0_ters_real(3)
   f0_ters_real(4)
   f0_ters_real(4)
   f0_ters_real(5)
```

```
   f0_ters_real(5)
   f0_ters_real(6)
   f0_ters_real(6)
   f0_ters_real(7)
   f0_ters_real(7)
   f0_ters_real(8)
   f0_ters_real(8)];
y=[ters_values_real(1)
   ters_values_real(1)
   ters_values_real(2)
   ters_values_real(2)
   ters_values_real(3)
   ters_values_real(3)
   ters_values_real(4)
   ters_values_real(4)
   ters_values_real(5)
   ters_values_real(5)
   ters_values_real(6)
   ters_values_real(6)
   ters_values_real(7)
   ters_values_real(7)
   ters_values_real(8)];
plot(x,y)
ylim([0 0.65])
xlabel('Frequency [Hz]')
ylabel('RMS Acceleration [m/s^2]')
title('Acceleration levels with a bandwidth of 5 Hz')
```

```
%%%%%%%%%%%%%%%%%%%%%%%%%%%%%%%%%%%%%%%%%%%%%%%%%%%%%%%%%%%%%%%%%%
% traped.m -Trapezoidal integration of vector y(x). 930203 S.D.Lee
%%%%%%%%%%%%%%%%%%%%%%%%%%%%%%%%%%%%%%%%%%%%%%%%%%%%%%%%%%%%%%%%%%

% Usage: f=traped(y,x) or f=traped(y)*dx, where y and x are both vectors.
% MATLAB routine f=ltitr(1,dx,y(:)) is less accurate.
function f=traped(y,x)
nr=length(y); dx=0*y;
if nargin==2, dx(2:nr)=diff(x); elseif nargin==1, x=[]; dx=dx+1; end
tmp=-y; tmp(2:nr)=y(1:nr-1); f=cumsum((y+tmp).*dx)/2;
% if (nargin==2) & (y(2)==0), f(1)=f(2); end
```

```
%%%%%%%%%%%%%%%%%%%%%%%%%
%mass-spring-damper system
%%%%%%%%%%%%%%%%%%%%%%%%%
clear all
close all
clc
t=linspace(0,60/60,10000);
A=1.5*10^-3;
Omega=60*2*pi;
m=7.5/1000; %mass [kg]
F_amp=0.7825; %[N]
x_amp=0.005; %[m]
c=F_amp/(x_amp*Omega);
xi=c/(2*m*Omega);
n=100;
step=(65-55)/n;

A=[0.005*10^-3 0.05*10^-3 0.5*10^-3 1*10^-3 1.5*10^-3];

for j=1:length(A)
    for k=1:n
        omega(k)=(55+(k*step))*2*pi;
        omega_d(k)=omega(k)*sqrt(1-xi^2);

        %% Maximum Power
        P_avg(j,k)=(m*xi*A(j)^2*(omega(k)/Omega)^3*omega(k)^3)/
        ((1-(omega(k)/Omega)^2)^2+(2*xi*omega(k)/Omega)^2);

        psi(k)=atan((2*xi*Omega*omega(k))/(omega(k)^2-Omega^2));
        lambda(k)=omega(k)^2/(sqrt((omega(k)^2-Omega^2)^2
        +4*xi^2*Omega^2*omega(k)^2));

        for i=1:length(t)
            z(k,i)=exp(-xi*omega(k)*t(i))*(lambda(k)*A(j)*Omega^2/omega(k)^2)
            *((1/omega_d(k)^2)*sin(omega_d(k)*t(i))*(Omega*cos(psi(k))-xi*
            omega(k)*sin(psi(k)))-cos(omega_d(k)*t(i))*sin(psi(k)))
            -(lambda(k)*A(j)*Omega^2/(omega(k)^2))*sin(Omega*t(i)-psi(k));
        end
        z_max(j,k)=max(abs(z(k,(9500:10000))))*1000; % [mm]
    end

end
```

```
%%%%%%%%%%%%%%%%%%%%%%%%%%%%%%%
%Fatigue Optimisation Algorithm
%%%%%%%%%%%%%%%%%%%%%%%%%%%%%%%
clc
clear all
close all

sigma_max=400e6;
L=linspace(40/1000,65/1000,1000000);
b=linspace(4/1000,8/1000,1000000);
h=linspace(0.4/1000,1.2/1000,1000000);
E=208.5e9;
m=7.5e-3;

freq=1;
b2=0;
L2=0;
h2=0;
b1=2;
for i=2:200

    while freq > 60.05 || freq < 59.95 || b1==b2(i-1)

        b1=b(randsample(length(b),1));
        h1=h(randsample(length(h),1));
        L1=L(randsample(length(L),1));
        I=b1*h1^3/12;

        freq=sqrt((3*E*I)/(m*(L1)^3))/(2*pi);
    end
    f(i)=freq;
    b2(i)=b1;
    L2(i)=L1;
    h2(i)=h1;
    A(i,:)=[b2(i) L2(i) h2(i)];

    p_max(i)=(2*(L2(i)^2)*sigma_max)/(3*E*h2(i));

end
```

B

Proof of Concept (In Swedish)

[redacted]

[redacted]

[redacted] – Beräkning av nyttig effekt avgiven från en ackumulerande rörelsepulsgenerator

Bakgrund

Ahlins Patentbyrå har genomfört och färdigställt en nyhetssökning med resultat som visar att uppfinningen är patenterbar.

STS Teknikskyddsgrupp har funnit att kommersiellt intresse för uppfinningen finns samt att företaget skall ansöka om patent om beräkningar kan styrka en nyttig och användbar funktion hos den i uppfinningsanmälan beskrivna principen. Detta för att säkerställa att principen håller för praktisk tillämpning i mobila system mm.

Metod

Den i [redacted] beskrivna principen bygger på Faradays lag om elektromagnetisk induktion samt Lenzs lag som beskriver den inducerade strömmens riktning motverkande den mekaniska rörelsen. Principen bygger också på harmonisk svängning samt systemets resonans. Detta tillsammans utgör en mycket komplex beräkningsmodell där en mängd indata saknas eller måste ansättas. För att undanröja samtliga osäkerheter har vi därför valt att utföra mätningar på en arbetande modell som har monterats på ett vibratorbord med känd ingångsrörelse. Den arbetande modellen är en första prototyp som vi själva tillverkat med minsta möjliga materialanskaffning och resursåtgång. Den skall ses som en demonstrator med syftet att kunna beräkna en avgiven nyttig effekt vid en viss exciterande rörelse. Det kvarstår naturligtvis ett stort utrymme för optimering som ytterligare kan höja verkningsgraden.

Resultat från mätningar på vibrator

Sinussvepning med vibrator visar att demonstratorn har en resonansfrekvens vid 29,7 Hz.

Vid randomvibration infaller denna frekvens periodiskt och demonstratorn sätts då i repetetivt återkommande självsvängning då den alstrar nyttig energi/effekt.

Sinusvibration 29,7 Hz ; 2,5g: (snäll vibration motsvarande yttre fordonsmiljö mm)

Demonstratorn, olastad, avger ca 20 V, växelspänning (peek to peek)

Inkoppling av likriktarbrygga med utjämningskondensator och last:

Demonstratorn avger vid lasten R = 180 Ohm en likspänning, U = 3,80 V och en likström, I = 20,9 mA

Beräkning av avgiven effekt

Effektlagen ger: **P = U x I** = 3,80 x 0,0209 = 0,0794 W, dvs 79,4 mW.

Relativ jämförelse med påtänkt framtida applikation, WDU (fordonsmonterad på MGS)

Den idag framtagna trådlösa laserdetektorn, WDU, är batteridriven och har en medelströmförbrukning på 0,8 mA vid 3,0 V (batterispänning). Detta ger en medeleffektförbrukning på 0,0024 W, dvs 2,4 mW.

Detta ger ett förhållande 33:1. Dvs Demonstratorn kan driva 33 st WDU:er helt utan batterier vid sinusvibration (29,7 Hz ; 2,5g).

Slutssats

Den arbetande modellen visar med stor säkerhet att nyttig effekt avges redan vid relativt låga vibrationsnivåer.
Det är bevisat att den i U-5065 beskrivna uppfinningen fungerar även i praktiken.

Bilagor

1. Bild, Demonstrator (arbetande modell)

2. Bild, Mätuppställning

3. Bild, Mätprotokoll

4. Bild, Demonstratorn driver 20 st LED:ar

Bilaga 1

Demonstratorns dimentioner:

Längd = 160mm
Höjd = 55mm
Djup = 27mm

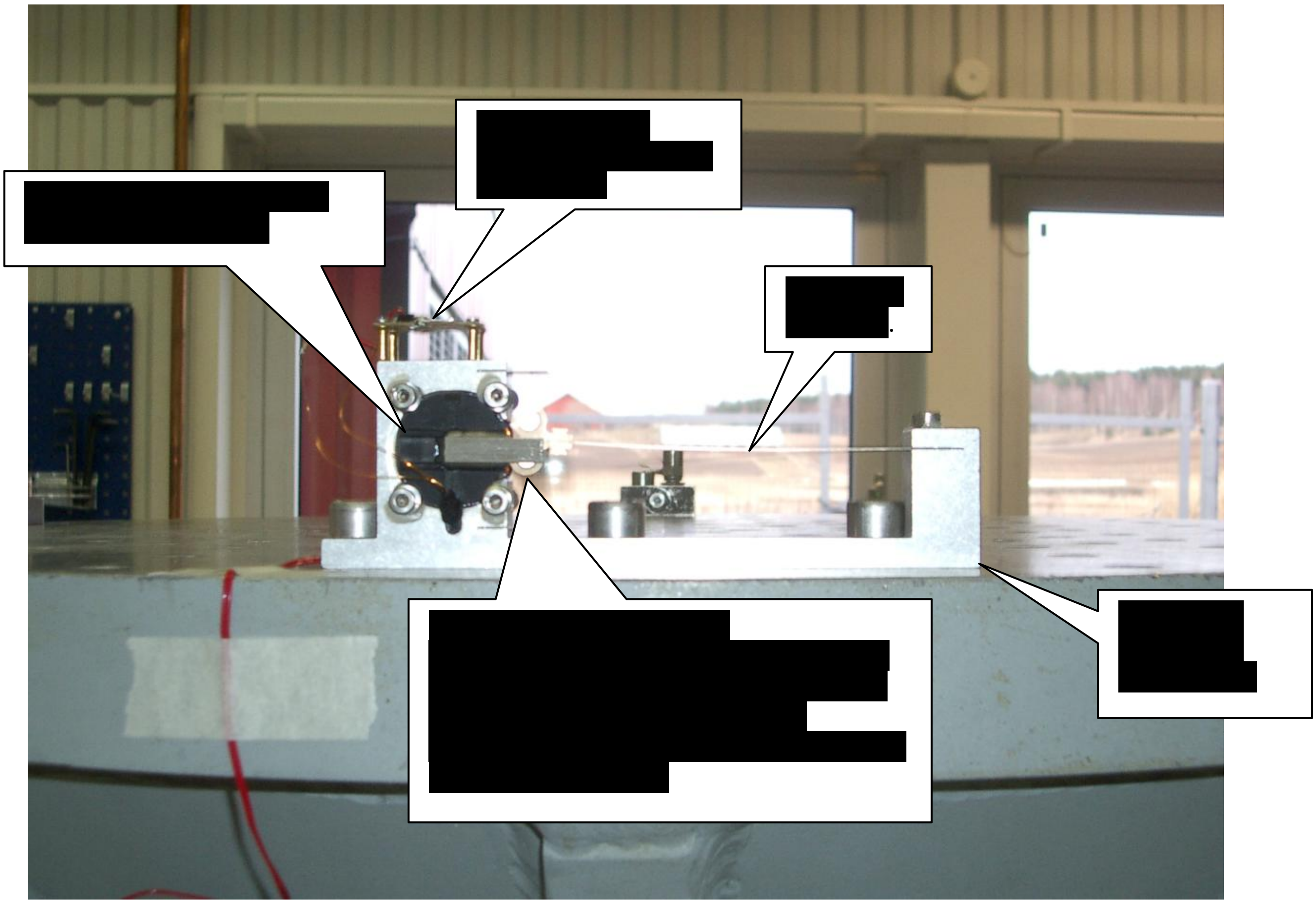

Figur 1. Arbetande modell/Demonstrator av en ackumulerande rörelsepulsgenerator, monterad på vibratorbord

Bilaga 2

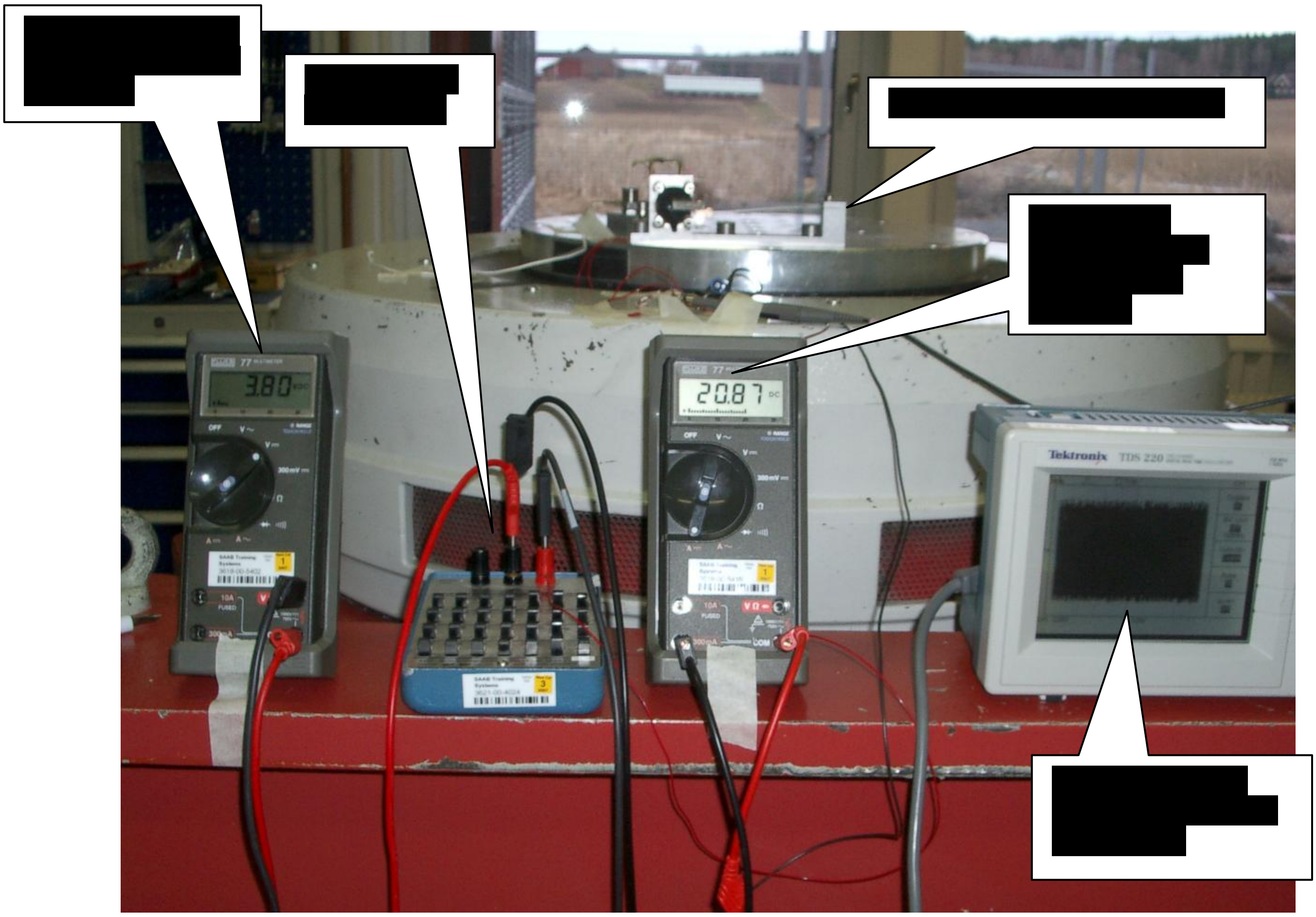

Figur2. Mätuppställning: Demonstrator med inkopplad last, Voltmeter, Amperemeter, Oscilloskop under pågående sinusvibration

Bilaga 3

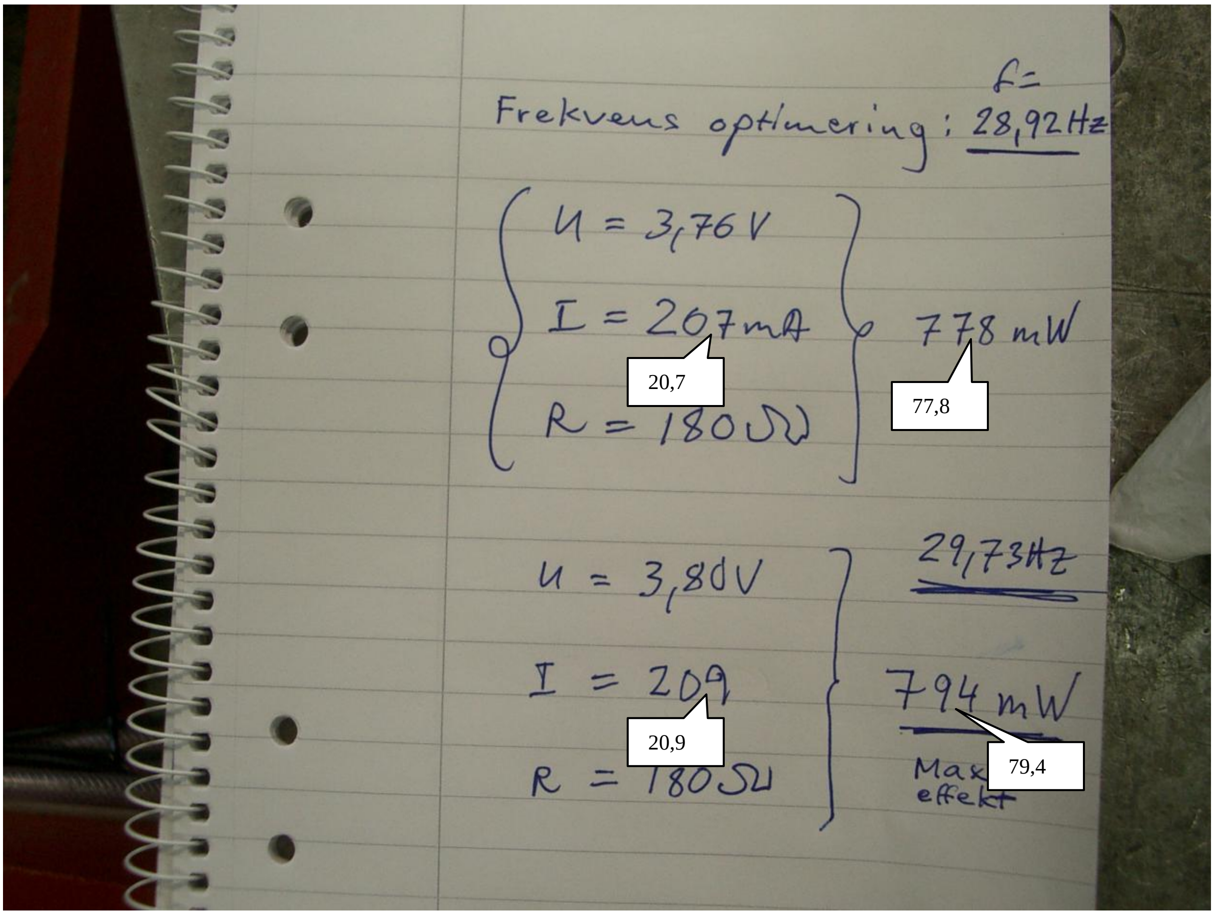

Figur3. Mätprotokoll: Avlästa världen under sinusvibration (f=29,7 Hz; 2,5g)

Bilaga 4

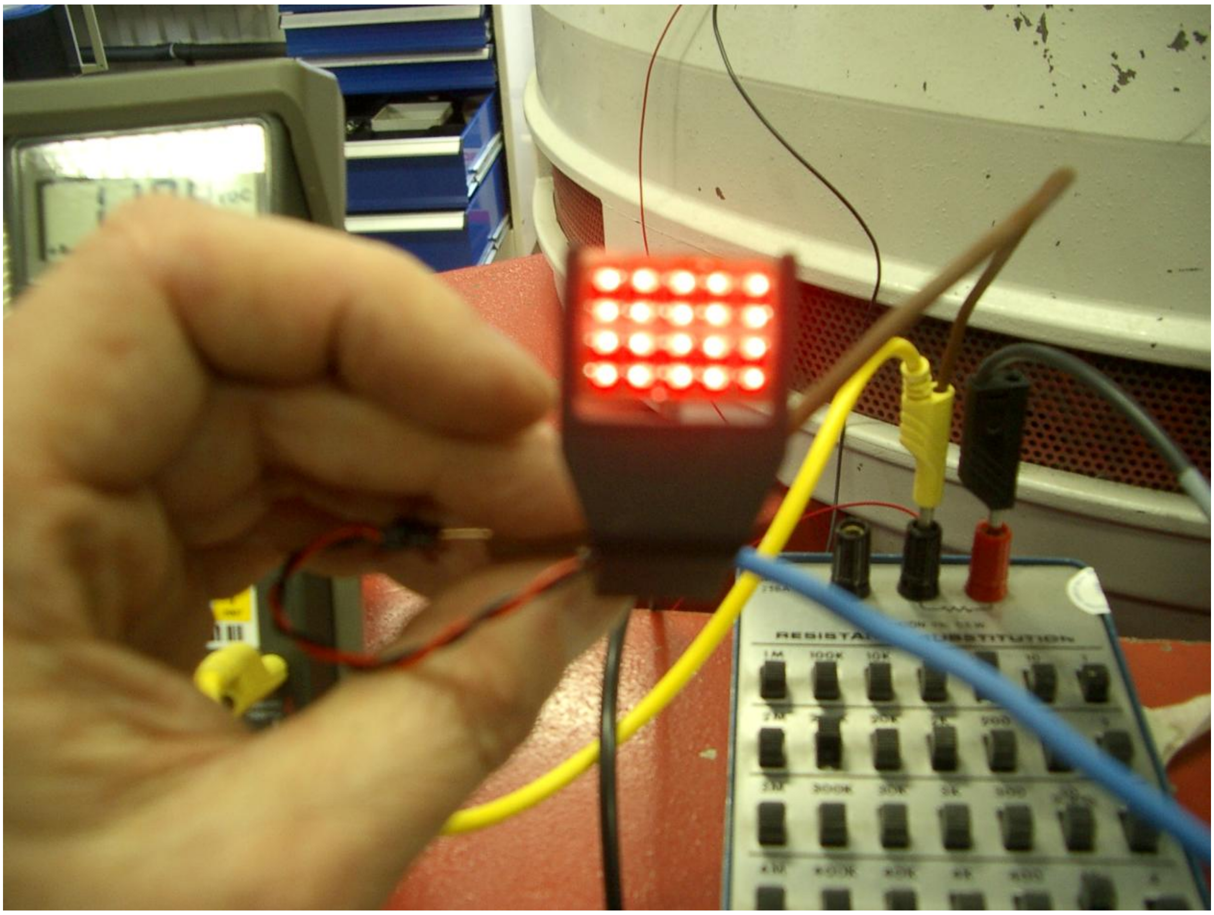

Figur4. Demonstratorn driver 20 st LED-ar som avger ett starkt rött sken, sinusvibration (f=29,7 Hz; 2,5g)

C

Specification from Upwis (In Swedish)

Resonansfrekvens: Resonansfrekvensen bör ligga på 60 Hz.

Effekt Min Krav: Bör under ett år kunna förse med samma energimäng som två AA batterier. Antag en batterikapacitet på 2000mAh, två batterier på totalt 2.5V vid belastning motsvarar då en total energi på ca 18 000 J. Under ett år skulle detta då motsvara en genomsnittlig effekt på 0.57 mW.

Form faktor: Nedan ges ett förslag på formfaktor, om någon dimension måste ökas för att uppfylla energikraven så bör harvesterns tjocklek ökas. Längd samt bredd kan anses som maximala mått. Om nedan angiven längd samt bredd används finns fyra reserverade områden i hörnen där det är tänkt att genomföringar för fastsättning bör ligga.

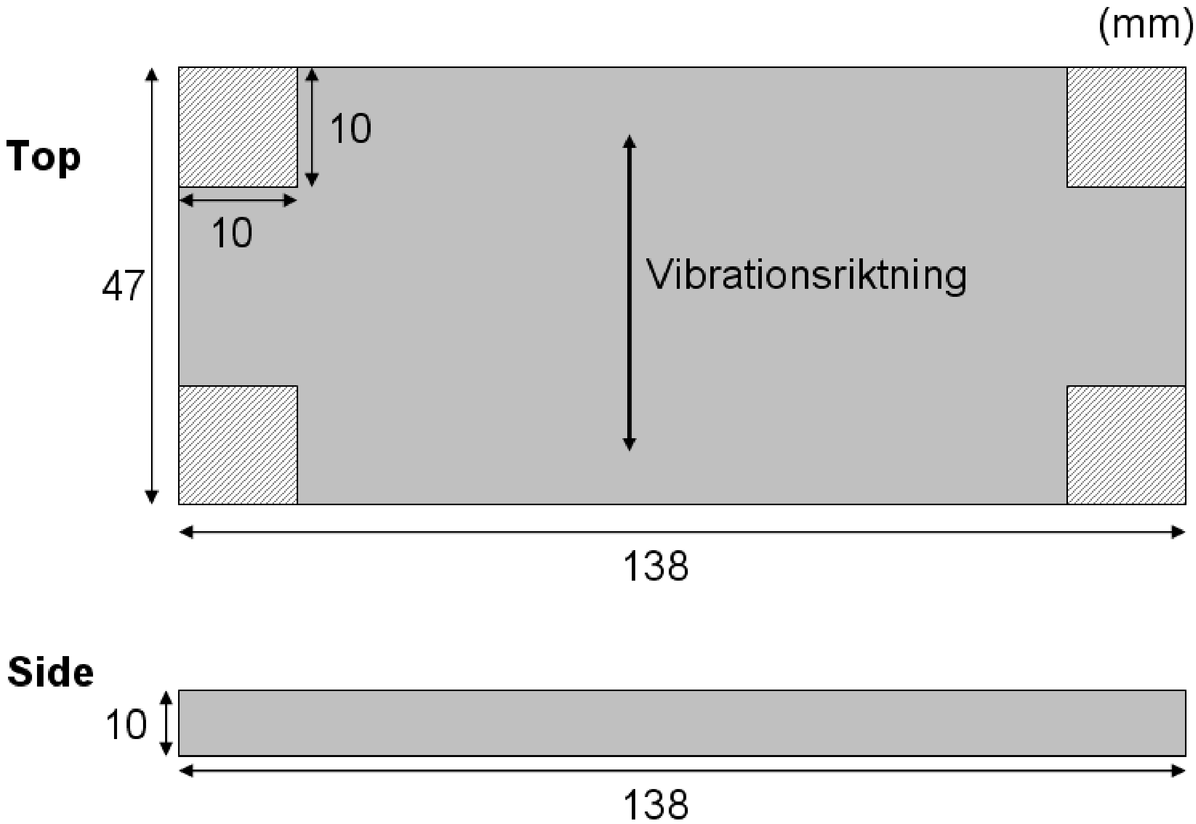

"Under ett år skulle detta då motsvara en genomsnittlig effekt på 0.57 mW " - gäller för sensorsystem med icke FFT beräkningar och runt 2% duty cycle, så kanske vi behöver lite mer som medeleffekt. Om man skall minska kostnader för mellanlagring (kondingar o mindre batteri) så är driftseffekten vid fullt spett på cpu ca 50-75mW - kan man önska så pass mycket så är det ju jättebra, kanske även realistiskt vid fullt skramlande godsvagn (5V 10mA peak)?

Just nu är kortdesignen anpassad för perpeetums generator, den har ca 5-10V AC utspänning, så då har jag optimerat systemlösningen internt så batteriladdare och nödladdning går mot 5V buss. (strömshuntladdare mot planerad 3.7-4.1V laddbar NimH eller LiPo ackumulator). Likriktare finns inne på kortet, så AC eller pulser går bra som inspänning - gärna 5V och uppåt.

D

Oscilloscope readings from test

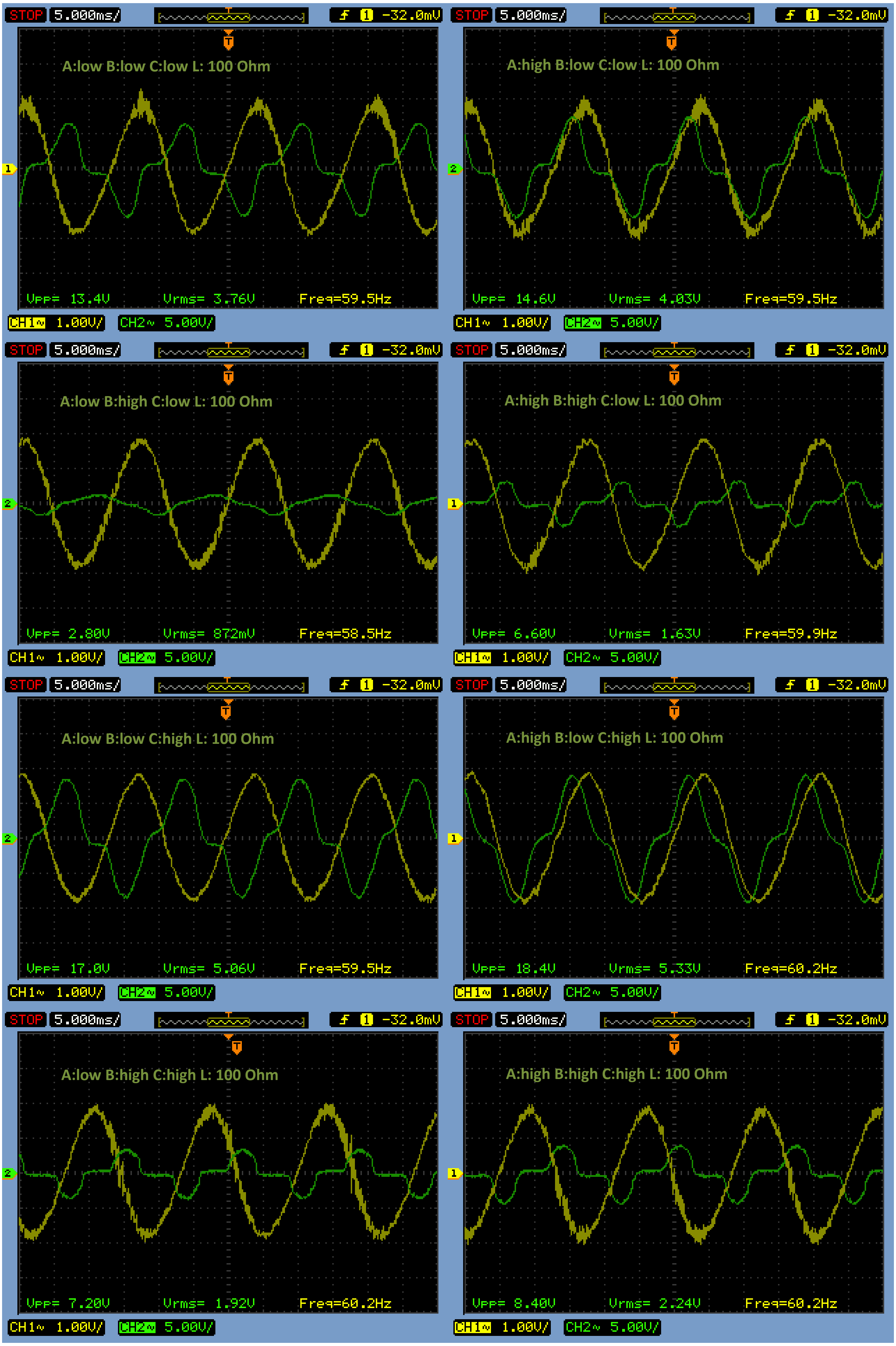
STOP 5.000ms/ -32.0mV
A:low B:low C:low L: 100 Ohm
Vpp= 13.4V Vrms= 3.76V Freq=59.5Hz
CH1 1.00V/ CH2 5.00V/
STOP 5.000ms/ -32.0mV
A:high B:low C:low L: 100 Ohm
Vpp= 14.6V Vrms= 4.03V Freq=59.5Hz
CH1 1.00V/ CH2 5.00V/
STOP 5.000ms/ -32.0mV
A:low B:high C:low L: 100 Ohm
Vpp= 2.80V Vrms= 872mV Freq=58.5Hz
CH1 1.00V/ CH2 5.00V/
STOP 5.000ms/ -32.0mV
A:high B:high C:low L: 100 Ohm
Vpp= 6.60V Vrms= 1.63V Freq=59.9Hz
CH1 1.00V/ CH2 5.00V/
STOP 5.000ms/ -32.0mV
A:low B:low C:high L: 100 Ohm
Vpp= 17.0V Vrms= 5.06V Freq=59.5Hz
CH1 1.00V/ CH2 5.00V/
STOP 5.000ms/ -32.0mV
A:high B:low C:high L: 100 Ohm
Vpp= 18.4V Vrms= 5.33V Freq=60.2Hz
CH1 1.00V/ CH2 5.00V/
STOP 5.000ms/ -32.0mV
A:low B:high C:high L: 100 Ohm
Vpp= 7.20V Vrms= 1.92V Freq=60.2Hz
CH1 1.00V/ CH2 5.00V/
STOP 5.000ms/ -32.0mV
A:high B:high C:high L: 100 Ohm
Vpp= 8.40V Vrms= 2.24V Freq=60.2Hz
CH1 1.00V/ CH2 5.00V/